Marine and Petroleum Geology 146 (2022) 105967

Contents lists available at ScienceDirect

Marine and Petroleum Geology

journal homepage: www.elsevier.com/locate/marpetgeo

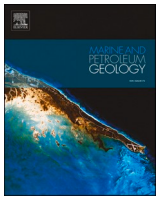

Diagenetic overprint on porosity and permeability of a combined conventional-unconventional reservoir: Insights from the Eocene pelagic limestones, Gulf of Suez, Egypt

Ahmed E. Radwan [a,*], Antun Husinec [b], Beatriz Benjumea [c], Ahmed A. Kassem [d], AK Abd El Aal [e,k], Mohammed Hail Hakimi [f,j], Hung Vo Thanh [g], Mohamed I. Abdel-Fattah [h], Amer A. Shehata [i]

[a] Faculty of Geography and Geology, Institute of Geological Sciences, Jagiellonian University, Gronostajowa 3a, 30-387, Kraków, Poland
[b] Department of Geology, St. Lawrence University, Canton, NY, 13617, USA
[c] Instituto Geológico y Minero de España, Madrid (IGME-CSIC), Spain
[d] Exploration Department, Gulf of Suez Petroleum Company (GUPCO), Egypt
[e] Department of Civil Engineering, Najran University, Najran, Saudi Arabia
[f] Geology Department, Faculty of Applied Science, Taiz University, 6803, Taiz, Yemen
[g] School of Earth and Environmental Sciences, Seoul National University, 1 Gwanak-ro, Gwanak-gu, Seoul, South Korea
[h] Petroleum Geosciences and Remote Sensing Program, Department of Applied Physics and Astronomy, University of Sharjah, Sharjah, 27272, United Arab Emirates
[i] Geology Department, Faculty of Science, Port Said University, Port Said, 42522, Egypt
[j] Department of Petroleum Engineering, Kazan Federal University, Kazan, 420008, Russia
[k] Geology Department, Faculty of Science, Al-Azhar University, (Assiut Branch), Assiut, Egypt

ARTICLE INFO

Keywords:
Thebes formation
Gulf of suez
Egypt
Eocene
October oil field
Porosity
Carbonate diagenesis
Petroleum
Asphaltene precipitation
Deep water pelagic limestones
Combined conventional-unconventioal reservoir

ABSTRACT

Lower to Middle Eocene organic-rich deep-water limestones of the ~335-m-thick (1100 ft) Radwany (Thebes-equivalent) Formation represent a source rock and a potential reservoir unit at the October Oil Field in the Gulf of Suez. However, in spite of recent exploration advances, the pore system and diagenetic history of the formation are still poorly understood. This study aims to discriminate porosity types and their vertical distribution, assess the diagenetic processes controlling porosity evolution, and evaluate the unit's overall reservoir potential. To achieve these goals, we utilized an integrated petrographic, mineralogical, geochemical and petrophysical dataset from four offshore wells. At October Oil Field, the Radwany Formation is informally divided into three intervals (from the base up: C, B and A) which are composed of planktonic foraminiferal wackestone, wackestone-packstone and packstone microfacies. Pores include both fabric selective (interparticle, intraparticle and moldic) and non-fabric selective (fracture) types. Visible porosity reaches up to 11.6%, and the highest porosity values are associated with interparticle pores in foraminiferal packstone in interval C. The two overlying intervals have lower porosities but have TOC values of up to 6 wt %. The Nuclear Magnetic Resonance (NMR) analysis yields low amplitudes of short T2 components (max. 52 ms), which suggests the presence of small pores (intraparticle, moldic, fracture, and fissure). Based on the electrical quality index (EQI) rock classification, nine groups were identified, suggesting a high heterogeneity of the formation. The highest EQI values positively correlate with high porosity (visible and estimated) in the lower part of Interval C which is dominated by interparticle/intraparticle porosity, thus reflecting the low tortuosity values of this microfacies. Dominantly low EQI values in Intervals A and B indicate low porosity efficiency and higher tortuosity. Carbonate sediments of the Radwany Formation are interpreted to have undergone a complex series of diagenetic processes. These processes modified the primary pore system either by enhancing the reservoir properties (dissolution and fracturing), or by reducing or destroying porosity (cementation, mechanical and chemical compaction, and minor pyritization, chertification, and asphaltene precipitation). The study highlights the unconventional reservoir potential of the middle and upper parts of the Radwany Formation (intervals B and A) at October Oil Field, and the conventional reservoir potential of interval C. It emphasizes the complexity of diagenetic controls on the porosity evolution in

* Corresponding author.
E-mail addresses: radwanae@yahoo.com, ahmed.radwan@uj.edu.pl (A.E. Radwan).

https://doi.org/10.1016/j.marpetgeo.2022.105967
Received 7 September 2022; Received in revised form 5 October 2022; Accepted 7 October 2022
Available online 13 October 2022

deep-water limestones of the Gulf of Suez, and may provide valuable insight into similar deep-water carbonate systems in rift basin reservoirs elsewhere.

1. Introduction

The petrophysical properties of carbonate rocks reflect both the original depositional processes and subsequent diagenetic modifications that may enhance and/or reduce porosity (Lucia, 2007). Following the syndepositional creation of primary porosity, which in modern carbonate sediments ranges from 40 to 70%, the reservoir properties of carbonates can be modified post-depositionally in eogenetic (near-surface and shallow burial), mesogenetic (deep burial), and telogenetic (uplift) realms (Choquette and Pray, 1970; Lucia, 2007). In carbonate reservoirs, porosity is commonly enhanced by dissolution and reduced by compaction and cementation, whereas recrystallization and

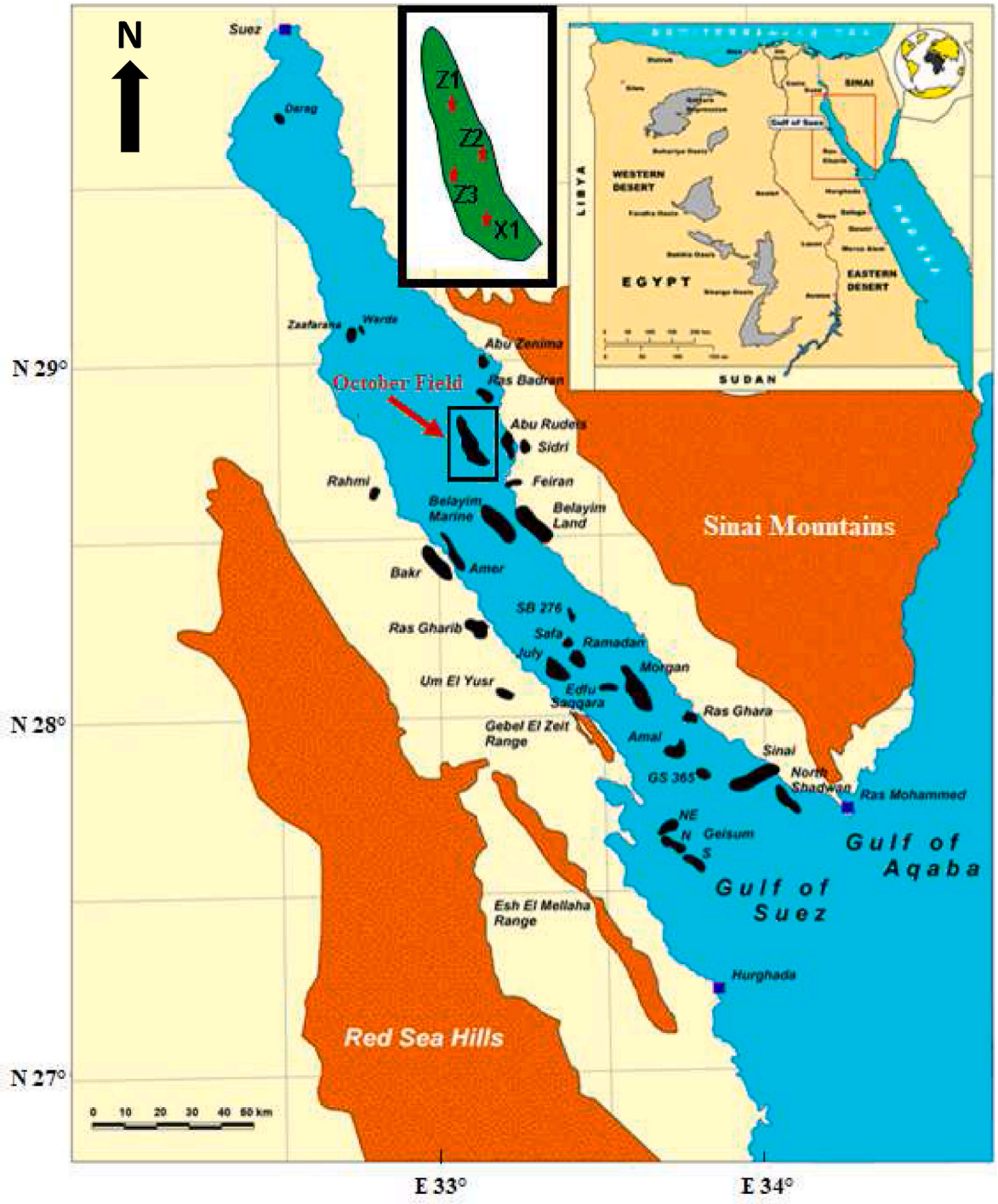

Fig. 1. Location map of oil fields in the Gulf of Suez region; the October Oil Field is marked with a black rectangle. The inset map shows the location of the study area in Egypt (modified after El Diasty et al., 2020).

replacement can both create and/or destroy porosity (Ahr, 2008). Fractures may significantly enhance porosity and permeability, but may also act as impediments to fluid flow if filled with gouge or mineral cements (Nelson, 2001). Consequently, complex pore systems are a characteristic feature of carbonate reservoirs, and nanno-to micro- and meter-scale pore connectivity can have a significant effect on hydrocarbon storage and recovery (e.g., Lomando, 1992; Hollis, 2011; Burchette, 2012; Ehrenberg et al., 2015; 2019; Hollis et al., 2017; Worden et al., 2018; Amel et al., 2015; Fallah-Bagtash et al., 2020; Kakemem et al., 2021; Ghasemi et al., 2022; Abouelresh et al., 2022). Thus, an understanding of the petrophysical properties of a carbonate reservoir is essential for reservoir evaluation (Benjumea et al., 2019; Boutaleb et al., 2022; Machel, 2005; Radwan et al., 2021a).

Due to the presence of more homogenous and easier-to-develop sandstone reservoirs, carbonate rocks in the Gulf of Suez subsurface have remained poorly studied and were not given the exploration priority in the past. This study focuses on the reservoir potential of the Ypresian to Lutetian (Lower to Middle Eocene) carbonate succession at the October Oil Field (Fig. 1). Lower to Middle Eocene carbonates in the Gulf of Suez and elsewhere in Egypt have conventionally been attributed to the Thebes Formation (e.g., Scheibner et al., 2001; Corlett et al., 2018). These grainy and nummulitic carbonates form a regionally extensive lithostratigraphic unit outcropping across Egypt, from the Western Desert and the Nile River Valley to the Eastern Desert and the Sinai Peninsula. The Thebes Formation carbonates were deposited in a relatively shallow-water platform setting along the southern Tethyan margin (Said, 1960; Shaaban, 2004; Guiraud et al., 2005). Recently, Radwan et al. (2020c) introduced a new formation name – Radwany Formation – for time-equivalent carbonates at the October Oil Field based on their interpreted deeper-water depositional environment and biostratigraphy. The petrophysical properties, diagenetic history, and reservoir potential of the Radwany Formation at the October Oil Field have previously not been investigated in detail. Based on its total organic carbon (TOC) content of 6 wt %, the formation has been identified as an oil-prone source rock in the October Oil Field area (El-Ghamri et al., 2002; Alsharhan, 2003; El-Shahat et al., 2009; Radwan et al., 2021a).

Here, we focus on the pore system network and the diagenetic overprint effects on porosity and permeability of the Radwany Formation in the October Oil Field, with a comprehensive evaluation of its reservoir properties based on an integrated lithofacies, mineralogical, geochemical, and petrophysical dataset. The results will help to improve understanding of the role and timing of diagenesis in modifying the reservoir potential, and provide new insights into producing strategies and the future exploration activities focused on the Eocene deep-water carbonates in the Gulf of Suez.

2. Geological setting

The NNW-SSE trending Gulf of Suez (Fig. 1) formed by rifting between the African and Arabian Plates (Said, 1962; Dolson, 2020) which was initiated at about 23 Ma (late Oligocene) (Robson, 1971; Mostafa et al., 1993; Patton et al., 1994; Alsharhan and Salah, 1994, 1995; McClay et al., 1998; Dolson et al., 2001). The basin is dominated by tilted fault blocks and half grabens bounded by normal faults (Patton et al., 1994; Dolson et al., 2014) and can be divided into three sub-basins that differ in terms of fault polarity and regional dip (Bosworth and Mcclay, 2001; Moustafa and Khalil, 2020). The northern and southern sub-basins show a regional SW dip, whereas the central sub-basin exhibits a NE dip (Patton et al., 1994). The sedimentary fill in the Gulf of Suez rift basin has been described by numerous authors (Said, 1962, 2017; Darwish and El-Araby, 1993; Attia et al., 2015; Abudeif et al., 2016, 2018; Radwan et al., 2019a, 2019b, 2019c, 2020a, 2020b, 2021b; Abdelghany et al., 2021; Radwan, 2021, 2022; Kassem et al., 2021) and can be divided into (i) a pre-rift succession which encompasses the deposits overlying Precambrian basement up to the rift initiation in the late Oligocene; (ii) a thick syn-rift (late Oligocene to late Miocene) succession, which is overlain by (iii) a post-rift (Pliocene to Holocene) succession. The October Oil Field (Fig. 1) is located in the north-central part of the rift basin, about 135 km SSW of the Suez City (28°46′40″N to 28°57′10″N, 32°57′33″E to 33°10′00″E) (Kassem et al., 2020; Radwan et al., 2020a,c; El Baz and Kassem, 2020; Shehata et al., 2021). The field covers an area of more than 22 km^2 and contains estimated ultimately recoverable reserves of about 725 MMbbl (millions of barrels) of oil (EGPC, 1996; El-Ghamri et al., 2002; Radwan et al., 2020c). The structural setting of the field is dominated by the NW-SE trending normal faults, and the associated pre-Miocene fault blocks that dip to the NE (Fig. 2) (EGPC, 1996; El-Ghamri et al., 2002; Kassem et al., 2020).

Production comes from siliciclastic reservoirs including the Palaeozoic-Lower Cretaceous Nubia Sandstone, the Upper Cretaceous Matulla, Wata and Raha Formations, and the lower Miocene Nukhul and Upper Rudeis Formations (Fig. 3). The oil-water contact was encountered at a depth of 3557 m (11,670 ft; true vertical depth sub-sea). Source rocks are the Campanian-Maastrichtian and Eocene carbonates, whereas the traps are structural and combined structural-stratigraphic (Kassem et al., 2020; El-Ghamri et al., 2002; El-Shahat et al., 2009).

The sedimentary succession in crestal wells at the October Oil Field is ~3000 m (9843 feet) thick (Fig. 3). The lower to middle Eocene carbonates of the Radwany Formation are dominated by planktonic foraminifera-rich limestones which are interpreted to have been deposited in a pelagic setting in water depths of several hundreds of meters (Radwan et al., 2020c). The formation conformably overlies the Paleocene Esna Formation and is unconformably overlain by Miocene shales and limestones (Fig. 4). Similar to the Esna Formation, the Eocene section thins on the eastern and western flanks of the field; the thinning seems to be a consequence of erosional rather than depositional processes.

3. Materials and methods

3.1. Core description and analyses

This study is based on the description and analysis of 300 feet (91.4 m) of side-wall cores from the OCT-X well and cuttings from wells OCT-Z1, -Z2, and -Z3 (Fig. 1). Formation top picks, formation thicknesses, and cuttings descriptions were conferred using the available composite mud logs and geological reports. The AAPG color scheme was used for the description of the cuttings and the sidewall core plugs. Thirteen sidewall core samples from the OCT-X well were used for petrographic, mineralogical, geochemical, and petrophysical analyses. Plug diameter was mostly 1.5 in (38 mm) and length was 4 in (101.6 mm), although some samples were ~3 in (76.2 mm) long after removing the material for thin sections and core analyses.

Standard petrographic analyses, point-counting, and visual porosity estimates were performed on 60 blue epoxy-impregnated thin sections (30 from well OCT-X, and 10 each from wells Z1, Z2, and Z3) at the laboratories of the Jagiellonian University, Poland and the Institute of Geology at the University of Innsbruck, Austria. Visual analyses included the identification of sedimentary structures along with Dunham's (1962) rock types, grain size and sorting, grain types and abundance, analyses of mineral (pyrite, chert) and asphaltene content, and fossil content. Mud-supported carbonate rocks containing more than 10% grains were identified as wackestones, whereas grain-supported rocks with micrite matrix were classified as packstones (Dunham, 1962). Where the rock texture was ambiguous, i.e. between mud- and grain-supported, the sample was referred to as a wackestone-packstone (average mud-content ~40%). Bioturbation intensity was defined using the modified Reineck (1963) scale (Taylor and Goldring, 1993). Sorting was described based on the visual comparison charts (Pettijohn et al., 1973).

Visible porosity was described using the Choquette and Pray (1970) classification scheme, and pore volume was calculated using the

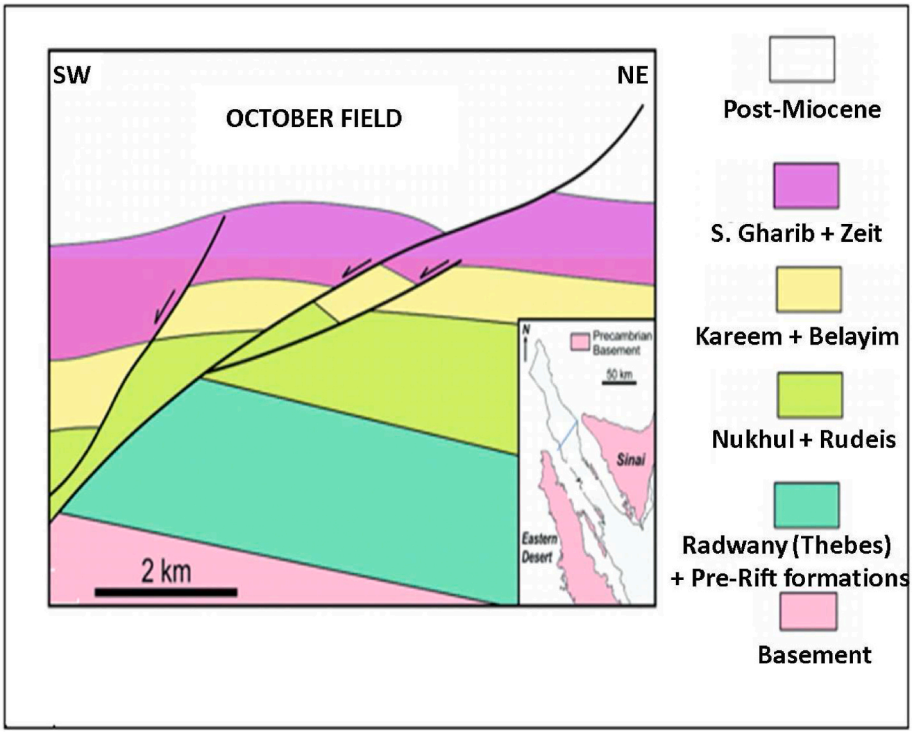

Fig. 2. Regional SW-NE cross-section through the central Gulf of Suez and October Oil Field showing the major structural features and the sedimentary succession overlying the Precambrian basement (modified after Moustafa and Khalil, 2020).

JMicroVision image analysis software on thin-section photomicrographs (Roduit, 2020). Porosity and permeability were measured on six sidewall core plugs (S1 to S6) using a helium gas expansion porosimeter (HEP-P) for porosity and the KA-210 gas permeameter for permeability.

3.2. Well-log analysis

Continuous gamma-ray (GR), density, neutron porosity, and resistivity logs of the studied Lower to Middle Eocene succession from the Oct-X well were analyzed. Petrophysical analysis focused on the comparison of continuous porosity values with lab measurements, total organic carbon (TOC) estimation, and rock classification into classes with similar petrophysical characteristics. Initially, during preprocessing of the well-log data, erroneous and invalid data were removed. The density porosity log was analyzed using density values of 2.72 g/cm^3 for the matrix and 1.1 g/cm^3 for the fluid. The matrix value is supported by six measurements in boreholes located in the area (Gupco, 2020). In addition, the effective porosity (Φ_e) was calculated from neutron porosity Φ_N and shale volume (V_{sh}) retrieved from the gamma-ray log:

$$\varnothing_e = \varnothing_N(1 - V_{sh}) \quad (1)$$

Given the little correlation between the compressional-wave (V_P) and shear-wave (V_S) velocity with depth or age in carbonates, they can be classified based on sonic measurements, mainly Vp/Vs ratio (e.g., Eberli et al., 2003). Since sonic log was not available, in our study we focused on the resistivity and porosity datasets, as they could be physically related to pore geometries (Soleymanzadeh et al., 2018).

These authors introduced the Electrical Quality Index (EQI) as a way of grouping rock samples based on the formation resistivity versus porosity relationship. The formation factor (F) is calculated as:

$$F = \frac{\rho_r}{\rho_f} \quad (2)$$

where ρ_r is the resistivity of the saturated rock, and ρ_f is the resistivity of the saturating fluid (the fluid resistivity was taken as 0.2 Ω m). The relationship between the formation factor (F) and the porosity (φ) was assumed to follow the Archie-Winsauer equation as:

$$F = a\,\varphi^{-m} \quad (3)$$

where m is the cementation factor and a is the tortuosity factor.

Soleymanzadeh et al. (2018) defined the EQI factor as:

$$EQI = \sqrt{\frac{1}{F\varnothing}} \quad (4)$$

where Φ is porosity which has been demonstrated as an effective parameter for petrophysical classification (Sun et al., 2021). The latter is based on the equivalency between the hydraulic and electrical tortuosities, as shown by Soleymanzadeh et al. (2018). EQI is inversely related to electrical tortuosity. Hence, using the EQI as an electrical rock-typing tool enables a petrophysical classification; in addition, such classification is controlled by microstructural parameters. We used the Soleymanzadeh et al. (2018) method, which included calculating EQI from the well logs, and obtaining the tortuosity (a) and cementation (m) factors for each of the EQI groups by fitting to the log-log plot. There is a positive relationship between the low porosity and moldic pore type with the high tortuosity factor, whereas the high porosity and connected pore types reduce the tortuosity factor (Soleymanzadeh et al., 2018).

3.3. NMR analysis

The Nuclear Magnetic Resonance (NMR) log evaluation is an important tool in petrophysical analysis of carbonate rocks (e.g., Westphal et al., 2005; Radwan et al., 2021a; Elsayed et al., 2022), as it is not influenced by the lithology. When used with the transverse-relaxation times (T2) and their distributions, it may be interpreted to give permeability, producible porosity, and irreducible water saturation (Gubelin and Boyd, 1997). NMR is also used in correlation and calibration of the permeability and porosity well-logs with core–plug petrophysical measurements and calculated water saturation, in which

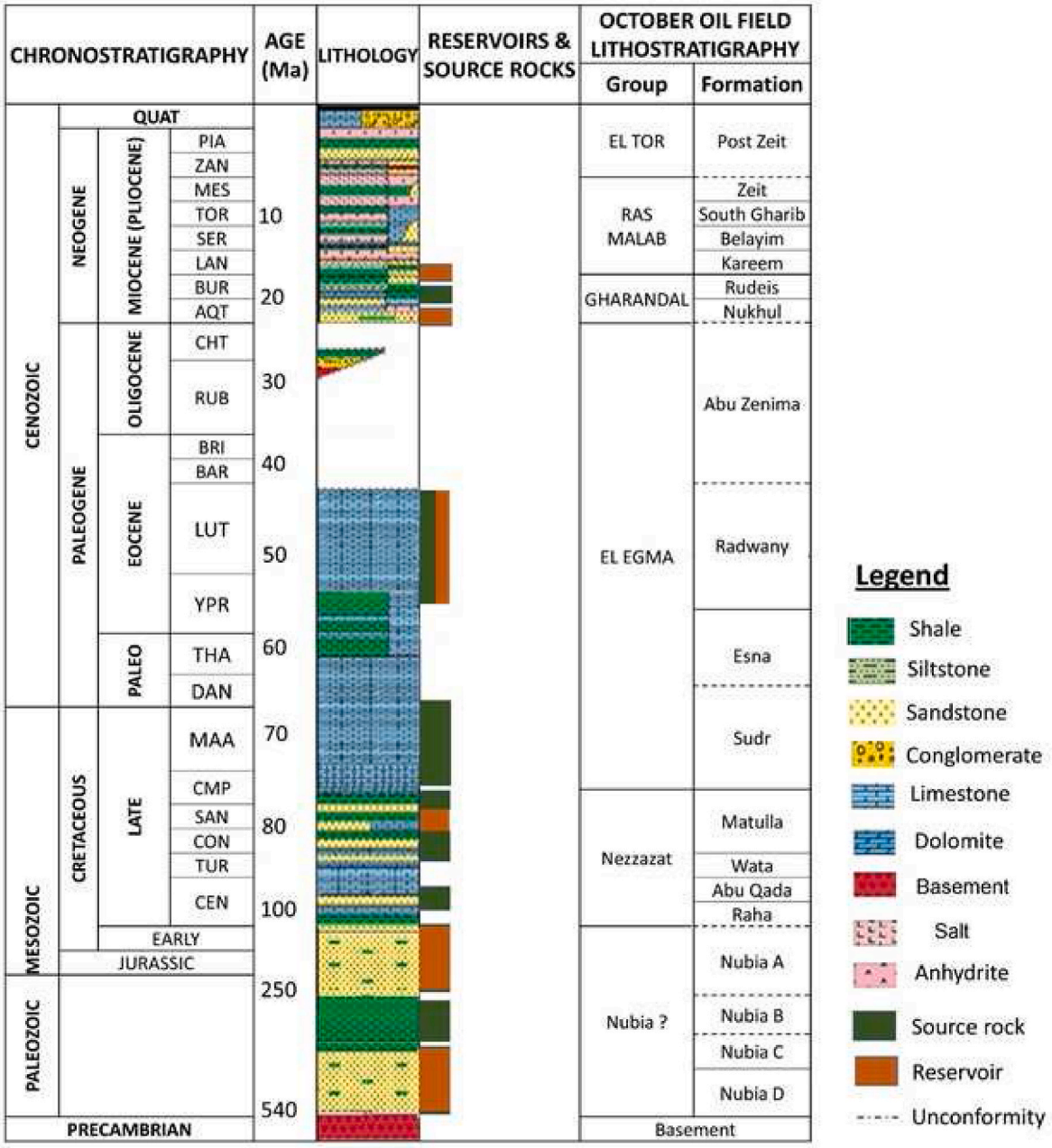

Fig. 3. Generalized stratigraphic column for the Gulf of Suez and the October Oil Field (Radwan et al., 2020c).

resistivity input is needed (Coates et al., 1999; Ehigie, 2010).

In this study, the porosity was analyzed using NMR on three samples (S1 to S3). A Carr-Purcell-Meiboom-Gill (CPMG) pulse sequence was used to measure the T2 distributions (Appel, 2004); WinDXP software (Resonance Instruments, UK) was utilized to obtain the T2 distributions from the CPMG echo-train data. The NMR log porosities were computed by inversion of the T2 distribution spectrum (Coates et al., 1999).

3.4. TOC analysis

TOC was measured on 10 samples of the Radwany Formation using a LECO CR-412 carbon analyzer at the Stratochem Laboratories, Egypt. Recently, advanced statistical methods were used to obtain TOC using geophysical well logging and lab measurements. However, these methods were limited to studies with a significant number of TOC measurements. Given the limited number of TOC values in this study, we have estimated a continuous TOC record of the studied interval by using the method of Zhao et al. (2016). It uses the overlap of density and neutron porosity difference (clay indicator, I_{cl}) and gamma-ray logs in a non-reservoir zone to obtain a separation between the two curves. The separation log is then correlated with TOC from sample analyses to obtain a continuous TOC log.

4. Results

4.1. Lithostratigraphy, mineralogical composition, and organic matter content

The thickness of the Eocene section in the October Oil Field varies in most wells from 918 feet (280 m) to 1050 feet (320 m), reaching a maximum of 1100 feet (~335 m) in the OCT-X well, the type well for the Radwany Formation (Radwan et al., 2020c) (Fig. 4). The succession is predominantly composed of massive, moderately burrowed, planktonic foraminifera-rich limestones whose color ranges from light to dark

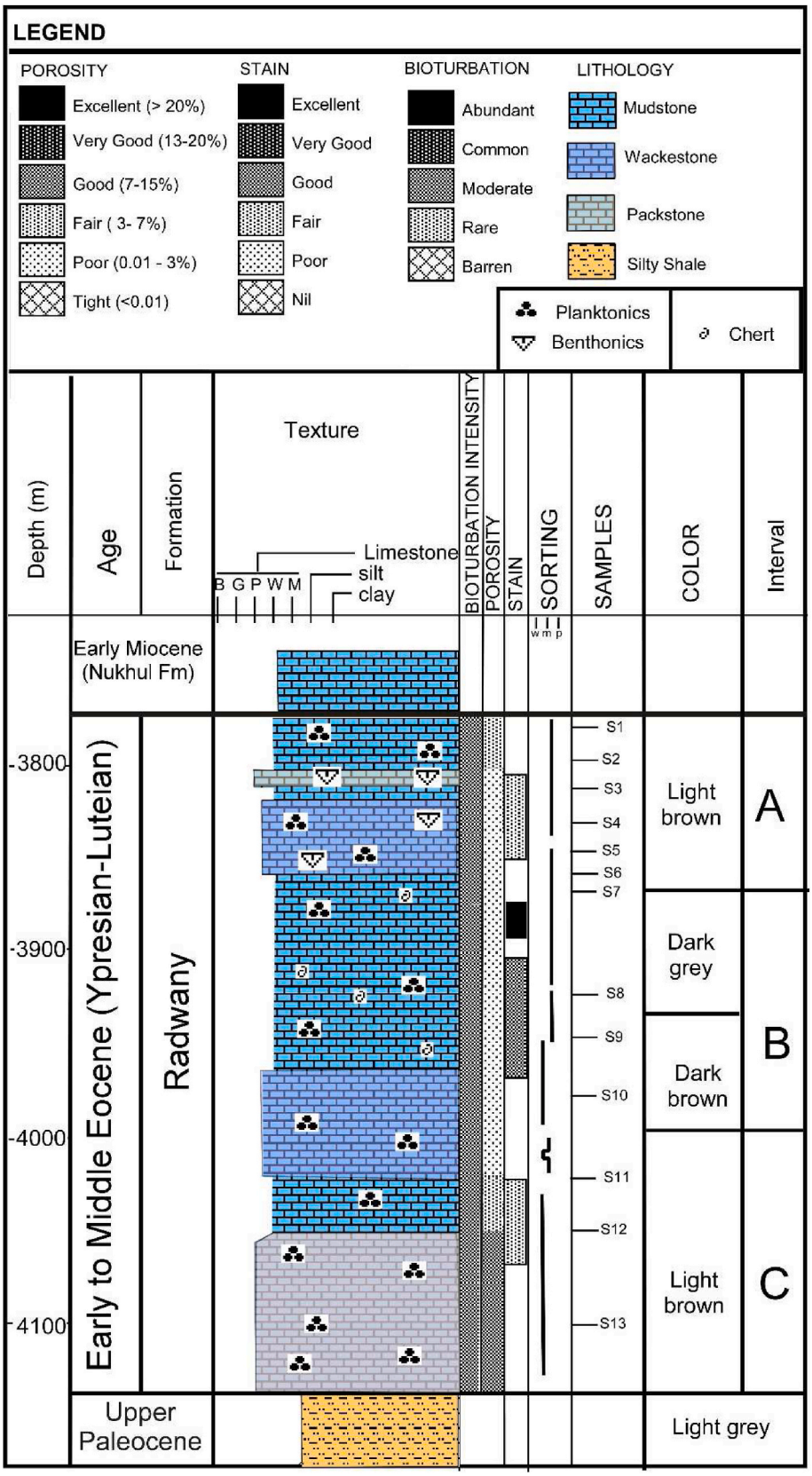

Fig. 4. Simplified stratigraphic column of the Radwany Formation at the OCT-X well, October Oil Field.

brown and dark grey, and with variable hardness as parts of the succession are chalky, slightly argillaceous, or contain chert (Fig. 4). Oil staining varies from fair to intense in samples from the upper part of the Radwany Formation, moderate in samples from the middle part, and fair in samples from the basal part.

The Radwany Formation at October Oil Field can be divided into three intervals based on microfacies (textural types), chert abundance, color, and detrital and authigenic components: these intervals, from the base up, are referred to here as C, B, and A (Fig. 4).

Interval C forms the lowermost ~130 m (427 ft) of the studied succession (Fig. 4). Mineralogically, the samples from this interval are dominated by calcite (89–92.5%) with rare pyrite (<1.3%) (Table 1, Fig. 5); chert is absent. The asphaltene content is up to 1% (mean 0.96%). Packstones are dominant in the lower part of the interval, wackestones in the middle, and wackestone-packstones in the upper part (Fig. 6).

Interval B forms the middle, ~100 m (328 ft) thick part of the studied succession (Fig. 4) and consists of wackestones (Fig. 6) with flattened pectens and planktonic foraminifera. In general, the interval is dark grey to dark brown and is characterized by the presence of chert fragments (up to 4.5%; mean 3.1%) and estimated clay content is 5%–11% (Table 1). The mean calcite content is 85.5% (maximum 86.5%), pyrite is rare (0.4–1.3%; mean 0.9%), and the average amorphous asphaltene content is 0.8% (maximum 1%) (Fig. 5).

Interval A forms the topmost ~105 m (345 ft) of the Radwany Formation (Fig. 4) and consists of wackestone-packstones and wackestones containing flattened pectens and planktonic foraminifera (Fig. 6). Interval A is pale brown and has a calcite content of 85.4%–91.8% (mean 89.9%), and mean clay content of 6.2% (4–9% range) (Fig. 5). The abundance of pyrite varies from 0.5% to 1.6% (mean 1.25%) and chert is absent. The amorphous asphaltene content varies from 0% to 0.8% (mean 0.34%).

4.2. Microfacies

Previous studies by Radwan et al. (2020c) have shown that the Radwany Formation at the October Oil Field is composed of three microfacies types: foraminiferal wackestones, wackestone-packstones, and packstones (Fig. 7). The carbonate textures and fossil content were interpreted to indicate a deep-water, outer ramp to basinal depositional setting. The rare occurrence of fine glauconite pellets (Fig. 8D) indicates a low depositional rate, although it is not clear if these pellets formed in situ (e.g., Föllmi and von Breymann, 1992) or were transported from the adjacent shallow shelf. Based on new information from the four wells analyzed in this study, the microfacies are summarized below.

4.3. Microfacies 1: foraminiferal wackestone

Planktonic foraminiferal wackestone makes up ~50% of the Radwany Formation and is the most abundant microfacies in interval B and parts of intervals C and A (Fig. 6). The microfacies is composed of microcrystalline calcite (micrite) and skeletal grains of predominantly small planktonic foraminifera (Fig. 7A and B), including keeled *Globorotalia* sp., deformed *Acarinina* sp. and *Morozovella* sp., along with globigerinoids and indeterminate biserial foraminifera. Other bioclastic grains include shell fragments (probably mollusks and ostracods) and echinoids. Samples of this microfacies have the lowest porosity values recorded in the Radwany Formation with secondary porosity, both fabric-selective moldic and not fabric selective (fracture), being the dominant type (Fig. 6).

4.4. Microfacies 2: foraminiferal wackestone-packstone

Foraminiferal wackestone-packstone forms parts of intervals C and A (Fig. 6). The main skeletal components are small planktonic and subordinate benthic foraminifera (Fig. 7C). Among the former, the most abundant are keeled *Globorotalia* sp., *Morozovella* sp., deformed *Acarinina* sp., and unidentified biserial species; deformed globigerinoids are subordinate. Open-marine benthic foraminifera include *Bolivina* sp. and *Bulimina* sp., both of which are commonly reworked. Other identified skeletal particles include bivalve and echinoid fragments. Similar to the foraminiferal wackestone, this microfacies is characterized by secondary porosity only. Moldic porosity dominates pore types in wacke-packstone in interval C, and both fracture and moldic porosity are present in interval A (Fig. 6).

4.5. Microfacies 3: foraminiferal packstone

Foraminiferal packstone makes up ~10% of the Radwany Formation in the October Oil Field. Bioclasts are represented by planktonic foraminifera, including keeled *Globorotalia* sp., *Morozovella* sp. and globigerinoids; benthic foraminifera are subordinate (Fig. 7D). Samples of this microfacies have the highest porosity values; pores include both fabric selective and non-fabric selective types. Interparticle primary porosity characterizes the microfacies in interval C, whereas fracture and moldic secondary porosity dominate in interval A.

4.6. Diagenetic features

The Radwany Formation underwent a complex diagenetic history, including shallow burial, late Eocene-early Oligocene uplift and erosion, and subsequent deep burial. Diagenetic processes included cementation, dissolution, mechanical and chemical compaction, pyritization, chertification, and hydrocarbon generation and migration (Fig. 6). Some of these processes have improved, whereas others have reduced the pore volume storage capacity and petrophysical properties of the studied succession.

Calcite cementation is ubiquitous throughout the Radwany Formation with drusy, blocky, and microcrystalline calcite cement types

Table 1
Gross mineralogy, OCT-X well, Radwany Formation, October Oil Field.

Interval	Depth (m)	Sample	Calcite (%)	Chert (%)	Clay (%)	Asphaltene-rich solids (%)	Pyrite (%)
A	3782	S1	90.5	0	9	0	0.5
	3794	S2	90.4	0	8	0.2	1.4
	3805	S3	85.39	0	7	0	1.6
	3818	S4	91.8	0	7	0.4	0.8
	3840	S5	91.02	0	5	0.2	1.6
	3852	S6	90.17	0	4	0.8	1.4
	3858	S7	90.12	0	4	0.8	1.5
B	3925	S8	86.48	3	7	1	1.3
	3949	S9	85.81	4.5	5	0.9	1
	3979	S10	84.36	2	11	0.5	0.4
C	4013	S11	92.2	0	3	1	1.2
	4050	S12	89.65	0	6	0.9	1
	4100	S13	92.48	0	4	1	1.26

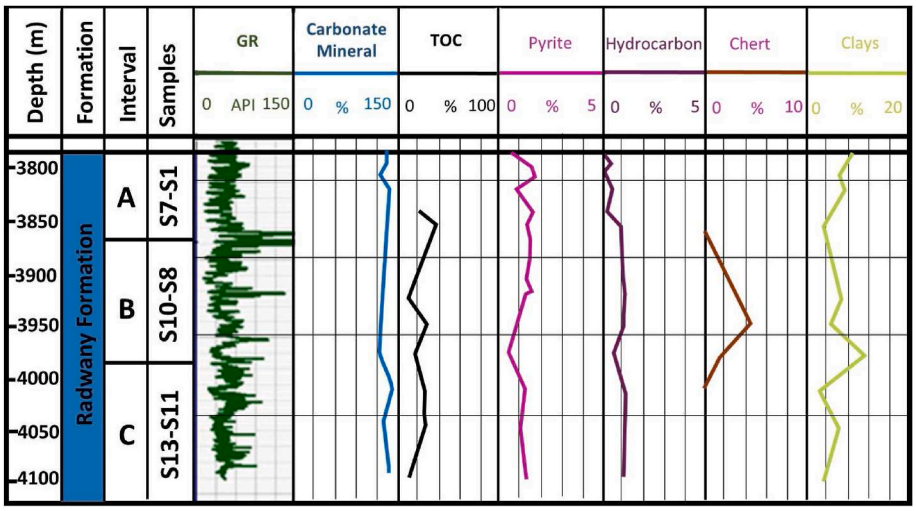

Fig. 5. Gamma-ray log, TOC, and gross mineralogy of the Radwany Formation measured on sidewall core samples, OCT-X well.

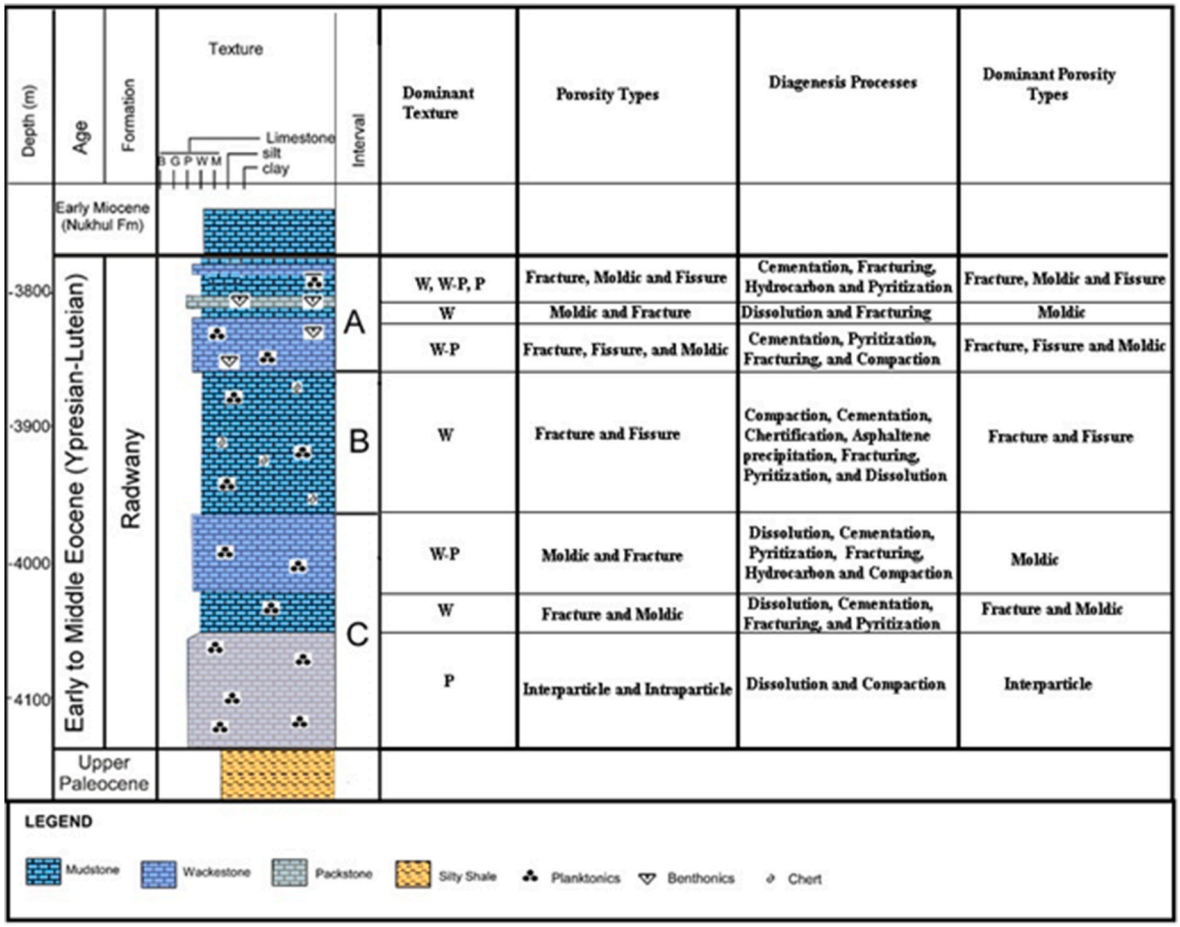

Fig. 6. Vertical distribution of microfacies, porosity types, and diagenetic processes in Intervals C, B, and A of the Radwany Formation, OCT-X well.

(Figs. 9 and 10). Drusy calcite cement fills intergranular and intraskeletal pores, molds, and fractures (Fig. 9 A, B) and is characterized by clear, euhedral to subhedral, equant to elongated crystals. Crystal size varies between 50 μm and 160 μm and crystals coarsen towards the center of void spaces. Less common are blocky spar and microsparite cements. Blocky spar fills fractures and locally occludes molds, whereas microsparite occurs as patches of very fine equant calcite crystals in the matrix of foraminiferal wackestone.

Dissolution is common in all three microfacies of the Radwany Formation and has primarily affected coarse bioclasts and foraminiferal tests resulting in the formation of moldic porosity. Due to differences in the size and shape of the affected skeletal material, the sizes of individual molds range from a few μm to several mm (Fig. 8F). Dissolution has also locally enlarged original interparticle and intraparticle pores as well as fractures.

Within the studied succession, mechanical compaction is commonly

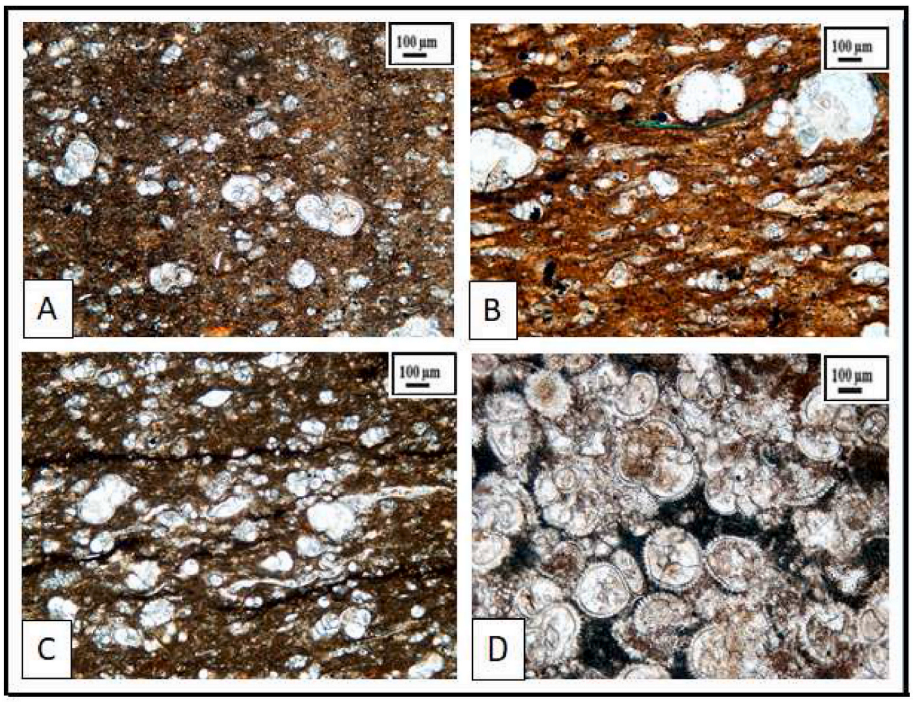

Fig. 7. Photomicrographs of carbonate microfacies in the Radwany Formation at the OCT-X well, October Oil Field. **(A)** planktonic foraminiferal wackestone with disseminated pyrite; depth 3955 m (12,976 ft). (**B**) planktonic foraminiferal wackestone; depth 3857 m (12,654 ft). (**C**) planktonic foraminiferal wackestone to packstone with fragmented bivalves and disseminated pyrite; depth 4000 m (13,123 ft). (**D**) planktonic foraminiferal packstone; depth 4065 m (13,337 ft).

observed in foraminiferal packstone where it is manifested as point-tangential and tight packing of the foraminiferal tests (Fig. 7D). Elsewhere in the section, mechanical compaction is indicated by the presence of deformed and broken bivalve shells that are closely packed. Wispy dissolution seams and stylolites (Figs. 9C and 10C), which in most cases are filled with dark brown asphaltenes, are evidence of chemical compaction (pressure solution) and are abundant throughout the formation.

Pyrite is present throughout the studied succession with the greatest abundance in intervals A and B (Fig. 5, Table 1), where it occurs in foraminiferal wackestone and wackestone-packstone. Pyrite occurs as microframboidal clusters or individual crystals dispersed in the micritic matrix or replacing larger bioclasts or foraminifera tests (Fig. 9E and F).

Chert has previously been recorded as a characteristic feature of the Eocene carbonates in Egypt, where it is typically found in well cuttings as cm-to m-thick angular fragments (Said, 1962, 2017; Abdel-Wahab and El-Younsy, 1999; Scheibner et al., 2001; Hussein and Abd El-Rahman, 2020). In the studied samples from the OCT-X well, chert fragments, most likely derived from nodules (cf., Hesse, 1989), were found exclusively in well cuttings from interval B foraminiferal wackestone (Figs. 4 and 5; Table 1).

Fractures and microfractures cut across the rock fabric in all three intervals of the Radwany Formation. Fractures are sinuous or branching (Fig. 9C and D, 11B), and are usually cemented with drusy calcite (Fig. 9 A, B) or filled with insoluble material or asphaltenes. Less commonly fractures are open and solution-enlarged (Fig. 8C). Both fractures and microfractures are most abundant in foraminiferal wackestone and wackestone-packstone.

Finally, the content of amorphous organic matter in the samples from the OCT-X well varies throughout the Radwany Formation. Organic matter abundance increases in foraminiferal wackestone and wackestone-packstone, and decreases in packstone. The dissolved compounds of crude oil (asphaltenes) are present in fractures and stylolites in foraminiferal wackestone-packstone and packstone (Fig. 9C and D, and 10; Table 2), and, in addition, some brown to black residual oil or tar is present locally.

4.7. Porosity types and distribution

Four types of porosity identified in the Radwany Formation are associated with both fabric selective (interparticle, intraparticle, and moldic) and non-fabric selective (fracture and fissure) pore types (Fig. 8).

Fabric selective porosity includes interparticle pores which are the dominant pore type in foraminiferal packstone in interval C (Fig. 8A), and occur less frequently in foraminiferal wackestone-packstone. The highest porosity values within the Radwany Formation (11.6%, Table 2) are associated with this porosity type. Intraparticle pores within benthic foraminifera and unidentified bioclasts contribute subordinately to the overall porosity in foraminiferal packstone and wackestone-packstone (Fig. 8A, E). The preferential dissolution of foraminifera and/or other bioclasts led to the development of irregularly shaped moldic spaces (Fig. 8F). Moldic porosity is common in intervals A and C, where it is most commonly associated with foraminiferal wackestone and wackestone-packstone (Fig. 6).

Non-fabric selective porosity includes fractures and fissures that cut across the rock fabric; fissures were distinguished from fractures based on their width of <10 μm and length of <1 mm. Fractures and fissures are ubiquitous in foraminiferal wackestone and wackestone-packstone, and occur throughout the Radwany Formation. They are observed at both the sidewall core and thin-section scales (Fig. 8B–D). Fracture porosity, although characterized by low values, enhances permeability by connecting other pore spaces together.

4.8. Porosity and permeability values

Porosity was calculated by both visual methods and laboratory measurements. In general, laboratory-measured values were higher because very small pore spaces are hard to identify by visual observation (Lucia, 2007).

(i) Visible porosity

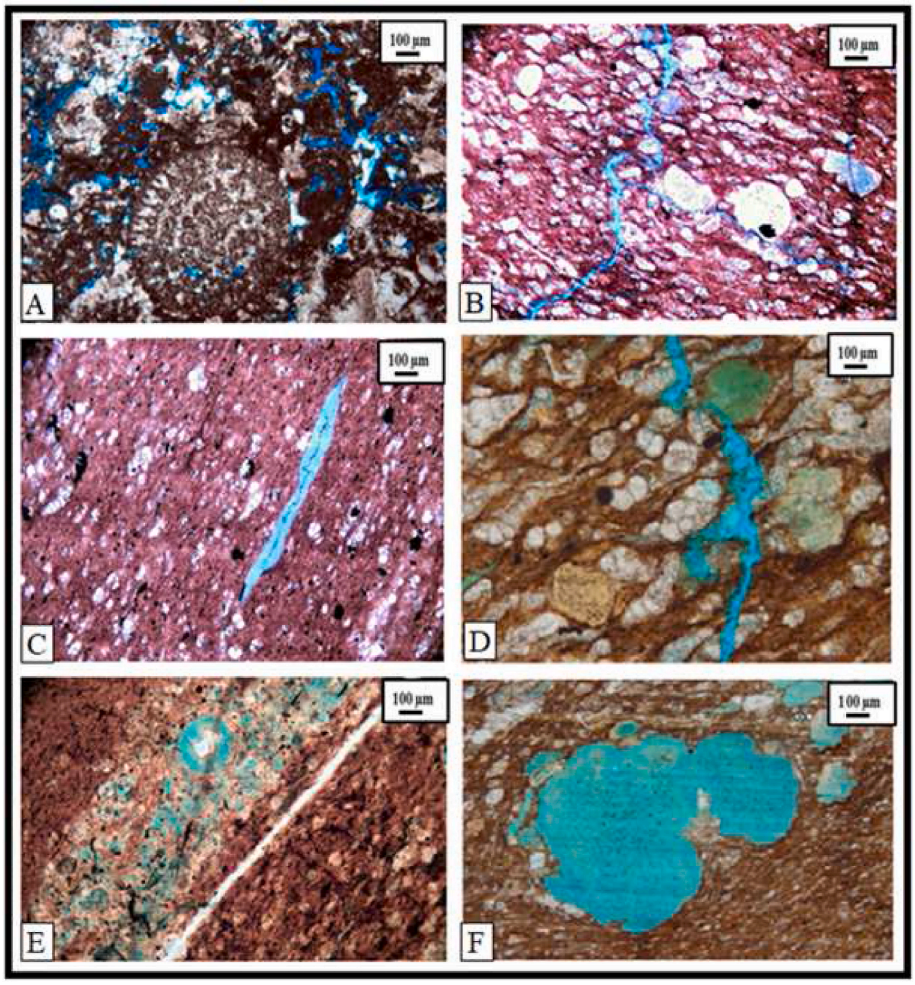

Fig. 8. Photomicrographs illustrating pore types in the Radwany Formation, October Oil Field; pores impregnated by blue epoxy. **(A)** intergranular and intragranular porosity within benthic foraminifera; Oct-X well, depth 4090 m (13,419 ft). **(B)** fracture porosity, sample depth 3870 m (12,697 ft), OCT-Z1 well. **(C)** Solution-enlarged fracture porosity, depth 3900 m (12,795 ft), OCT-X well. **(D)** Fracture porosity, depth 3915 m, OCT-Z2 well. **(E)** Intragranular porosity; depth 4000 m (13,123 ft). **(F)** Moldic porosity, depth 3885 m (12,746 ft), OCT-X well. (For interpretation of the references to color in this figure legend, the reader is referred to the Web version of this article.)

Visible porosity throughout the studied succession reaches up to 11.6% (mean 2.5%; Fig. 11, Table 2). The lowest values characterize foraminiferal wackestone in interval B (0.3–1%). Foraminiferal packstone and wackestone-packstone in interval B exhibit >4x greater mean porosity (1.7%) with values ranging between 1% and 4%. The highest porosity values were recorded in interval C where the foraminiferal packstones have a porosity of up to 11.6% (mean 10.2%). Residual hydrocarbons plugging the small pores and wispy dissolution seams are common (Figs. 9 and 10).

(ii) Core-plug porosity and permeability

A limited set of data from sidewall core plugs from the upper part of the Radwany Formation (interval A) shows little variation in porosity and permeability values between the different microfacies. Measured porosity ranges from 0.6% to 1% (mean 0.85%), and the very low permeability values range between 0.0009 mD and 0.0093 mD (mean 0.0044 mD) (Table 2, Fig. 12).

(iii) Nuclear Magnetic Resonance (NMR) porosity

All three samples analyzed contained exclusively secondary pores (fracture and moldic). The mean transverse relaxation time (T2) for the two samples of foraminiferal wackestone were 2.21 ms and 49.4 ms, which corresponds to NMR porosities of 7.7 pu and 13.8 pu, respectively. Slightly higher T2 values (mean 52.6 ms) characterized the foraminiferal packstone, with NMR porosity of 10.4 pu (Table 2, Fig. 13). The T2 spectra exhibit a bimodal left-skewed distribution (Fig. 13). The low amplitudes of short T2 components (Table 2) suggest the presence of small pores (intraparticle, moldic, fracture, and fissure). Overall, the NMR porosity values are higher than the core-plug porosity measurements (Table 2). According to Aqel (2016), the laboratory-measured porosity values for lower permeability rocks are lower than their NMR porosities.

(iv) Wireline log-based porosity

Based on the petrophysical evaluation of the density and neutron logs, the estimated mean effective porosity of the Radwany Formation carbonates is 10% (Table 2, Fig. 14). Similar to the visible porosity, the wireline log-based estimated effective porosity shows the lowest values within the foraminiferal wackestone in interval B (minimum 2%, mean 8%) (Fig. 14). Porosity values of interval A (foraminiferal wackestone and wackestone-packstone) vary across the interval (Fig. 14), whereas foraminiferal packstone in interval C has the highest effective porosity of up to 15% (mean 9.5%).

4.9. EQI-based rock classification

EQI was calculated by utilizing the geophysical well-log data in equations (2)–(4). EQI variation with depth is shown in Fig. 14, whereas Table 3 shows values of tortuosity and cementation factors obtained from the linear fitting of the log-log plot of formation factor versus porosity (Fig. 15). The highest EQI values characterize the lower part of Interval C, which is dominated by interparticle/intraparticle porosity. The remaining parts of Interval C with fracture-moldic (middle part) and

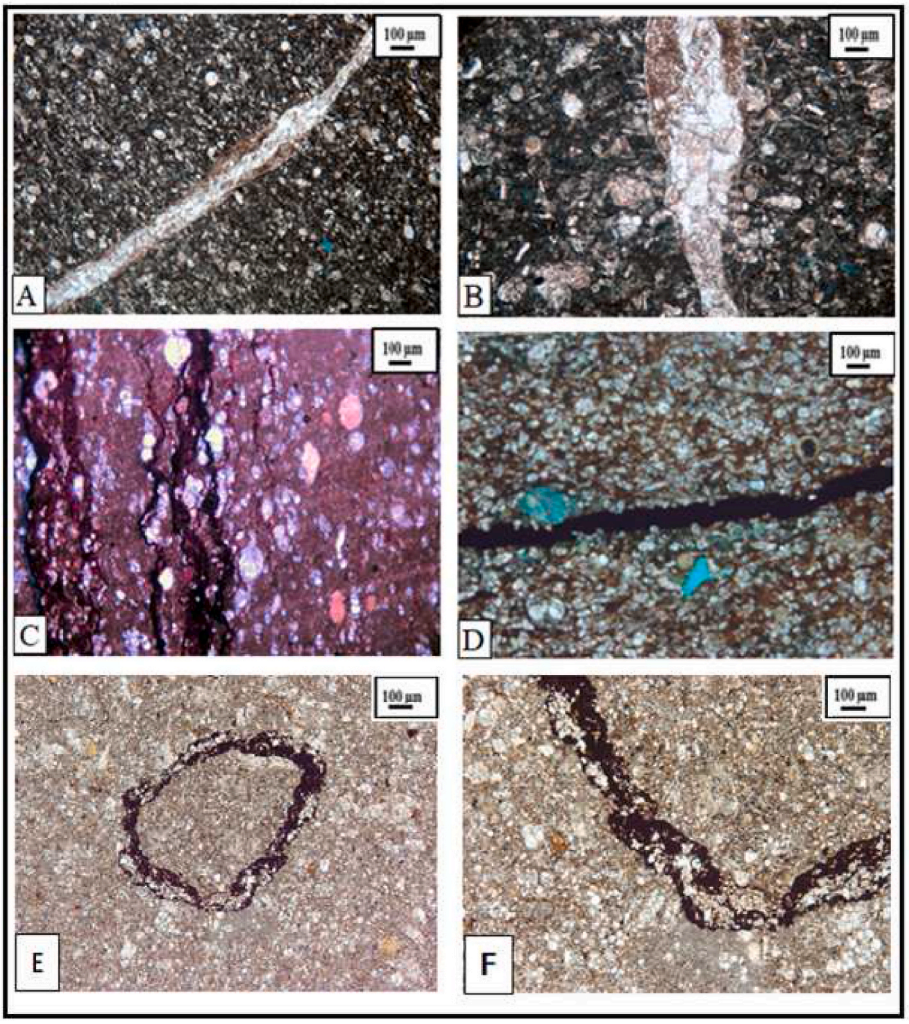

Fig. 9. Photomicrographs illustrating diagenetic features of the Radwany Formation, OCT-X well, October Oil Field. **(A-B)** fissure-filling drusy calcite, depth 3900 m (12,795 ft) in A, and 4000 m (13,123 ft) in B. **(C)** Wispy dissolution seams filled with asphaltene; depth 3970 m (13,025 ft). **(D)** Asphaltene-filled fissure (black), depth 3885 m (12,746 ft). **(E-F)** Pyrite replacing larger bioclasts, depth 3920 m (12,861 ft).

moldic-fracture porosities (upper part) exhibit low to moderate EQI values. Interval B with fracture-fissure porosities shows overall the lowest EQI values, albeit moderate values (0.3–0.5) were recorded in a few intervals. Low values of EQI predominate in the lower and middle part of interval A that are characterized by moldic and fracture fissure porosities (Fig. 14), whereas its upper part with fracture-moldic-fissure porosities has moderate values (0.3–0.5).

4.10. TOC distribution

The measured TOC values of the Radwany Formation range from 1.22 to 6 wt % (Table 2). The highest mean TOC value is in Interval A (3.85 wt %), followed by Interval C (2.6 wt %), and Interval B (1.9 wt %) (Table 2). The continuous estimated TOC log (Fig. 14) generally shows a very good correlation with the core-measured TOC values; only one outlier in the upper part of Interval A poorly correlates. The well log-estimated TOC in Interval C ranges between 1 wt % and 3 wt % (maximum <4 wt %: Fig. 5), and exhibits a close correlation with core-measured values (Fig. 14). In Interval B, the well log-estimated TOC generally ranges between 1 wt % and 2 wt %, with three intervals exceeding 3 wt % (maximum 4 wt %). Well log-estimated TOC in Interval A is higher in the lower part (maximum 5 wt %), and lower in the upper part (mostly 0.5–2 wt %).

5. Discussion

5.1. Diagenetic overprint on porosity and permeability

The predominance of secondary pore types (moldic, fissure, and fracture) indicates a complex, multi-stage diagenetic history of the studied succession, which took place over a range of diagenetic settings (Fig. 16). The studied ~335 m (1100 ft) thick lower (Ypresian) to middle Eocene (Lutetian) succession at the October Oil Field was formed by the slow deposition of carbonate mud and pelagic foraminifera in a deep-water setting with limited terrigenous influence, as evidenced by the relatively low clay mineral content (Table 1). Following deposition, the Eocene carbonates underwent a series of diagenetic processes including fracturing which modified the primary pore system. Some processes improved the reservoir properties (e.g., dissolution and fracturing) while others reduced them by plugging the voids and pore spaces (e.g., cementation, mechanical and chemical compaction, and hydrocarbon migration; subordinate chertification and pyritization). Based on the overall porosity and permeability values, the Radwany Formation may be considered as relatively tight.

5.1.1. Porosity-enhancing diagenetic processes

Solution-enlarged porosity includes fine-scale inter- and intraparticle pores and molds. Dissolution contributed to the creation of pore spaces

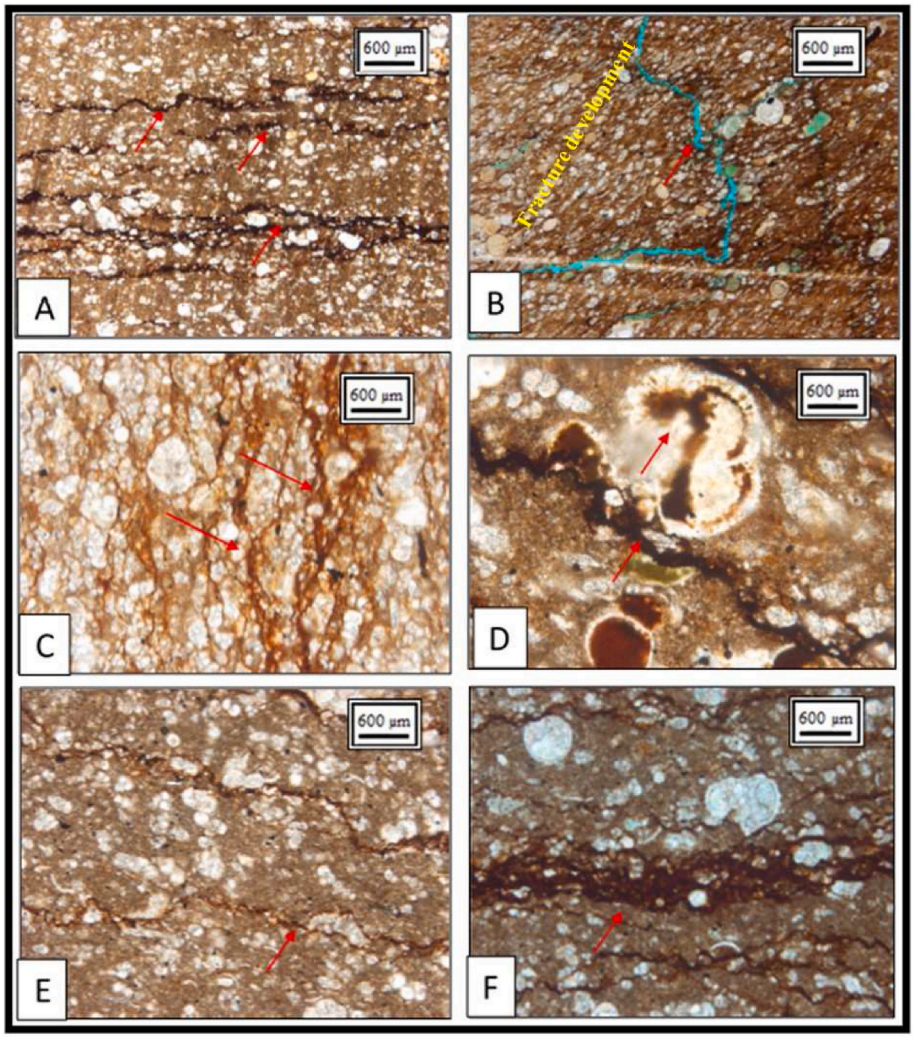

Fig. 10. Photomicrographs illustrating late diagenetic features of the Radwany Formation (indicated by red arrows): **(A)** Asphaltene-filled microstylolites; depth 3800 m (12,467 ft), OCT-Z1 well. **(B)** Open sinuous fissure; depth 3850 m (12,631 ft), OCT-Z2 well. **(C)** Asphaltene-filled wispy dissolution seams; depth 3910 m (12,828 ft), OCT-Z3 well. **(D)** Asphaltene-filled foraminiferal mold and microstylolite; depth 3870 m (12,697 ft), OCT-Z2 well. **(E)** Asphaltene-filled microstylolites, depth 3910 m (12,828 ft), OCT-X well. **(F)** Asphaltene-filled wispy dissolution seam. Note blocky spar-filled *Globogerinoides* sp. cast above; depth 3910 m (12,828 ft), OCT-Z1 well. (For interpretation of the references to color in this figure legend, the reader is referred to the Web version of this article.)

during early burial, uplift, and continued later, as aggressive pore fluids migrated laterally and vertically through the formation (Fig. 8F). Acids were likely formed during the thermal maturation of organic matter (Tucker and Wright, 1990), and may also have been generated during sulfate reduction that resulted in hydrogen sulfide generation and the precipitation of pyrite (Machel, 2001; Biehl et al., 2016). Overall, the leaching of grains and/or matrix played a moderate role in the creation of pore spaces (cf., Moore, 2001; Ehrenberg et al., 2012).

Strong post-Ypresian tectonic movements characterize the geodynamic history of present-day Egypt, including the Gulf of Suez (Patton et al., 1994; Bosworth et al., 2014). The present-day structural style of the October Oil Field area was shaped immediately before or during the Miocene, and early Miocene extension was associated with rapid subsidence, fault-block rotation, and marine transgression (Steckler et al., 1988; McClay et al., 1998; El-Ghamri et al., 2002) as well as significant fracturing of the Eocene carbonate succession. In addition, some fracturing may also be the result of the late Eocene N–S to NW–SE directed compression (Bosworth et al., 2014).

The fractures and micro-fractures identified in sidewall core samples, cuttings, and thin sections from the Radwany Formation at the October Oil Field indicate that brittle deformation had a significant impact on the creation of pore space and hydrocarbon migration pathways (Bastesen and Rotevatn, 2012; Rotevatn and Bastesen, 2014) (Fig. 8B–D). Some fractures were enlarged by dissolution (Fig. 8C), which lead to better connectivity between separate vugs and molds and, subsequently, an enhanced permeability. However, during late burial, most of the observed fractures were filled with calcite cement or asphaltenes, which resulted in reduced porosity and limited the positive impact of fracturing on reservoir quality. Hairline-thin fissures are filled with drusy calcite cement, whereas coarse blocky calcite occludes wider fractures. In addition, most fissures appear to be poorly connected as evidenced by the low permeability values of densely fissured intervals.

5.1.2. *Porosity-reducing diagenetic processes*

5.1.2.1. Cementation. Cementation reduces both primary and secondary porosity as pore spaces become filled with carbonate and other authigenic cements (e.g., Lucia, 2007; Ehrenberg and Walderhaug, 2015; Al-Ramadan et al., 2020; Abdullah et al., 2022; Boutaleb et al., 2022). It is ubiquitous in intermediate and deep-burial settings of elevated temperatures, fluid mixing, and chemical compaction, where it is associated with significant porosity/permeability reduction (e.g., Montañez et al., 1997; Machel, 2005; Read et al., 2016). Within the studied succession, the preservation of burrows, absence of lamination, and presence of intervals with intact foraminiferal tests, some of which contain calcite overgrowths, suggest that the precursor carbonate muds were deposited at slow rates and underwent at least some early lithification (cf., Fischer and Garrison, 1967; Bartlett and Greggs, 1969; Matter et al., 1975). However, given the general absence of early calcite cements, pressure solution was likely a major source of calcium ions once pore waters had been expelled during burial-related compaction. Thus, microcrystalline spar likely pre-dates the mold- and fissure-filling

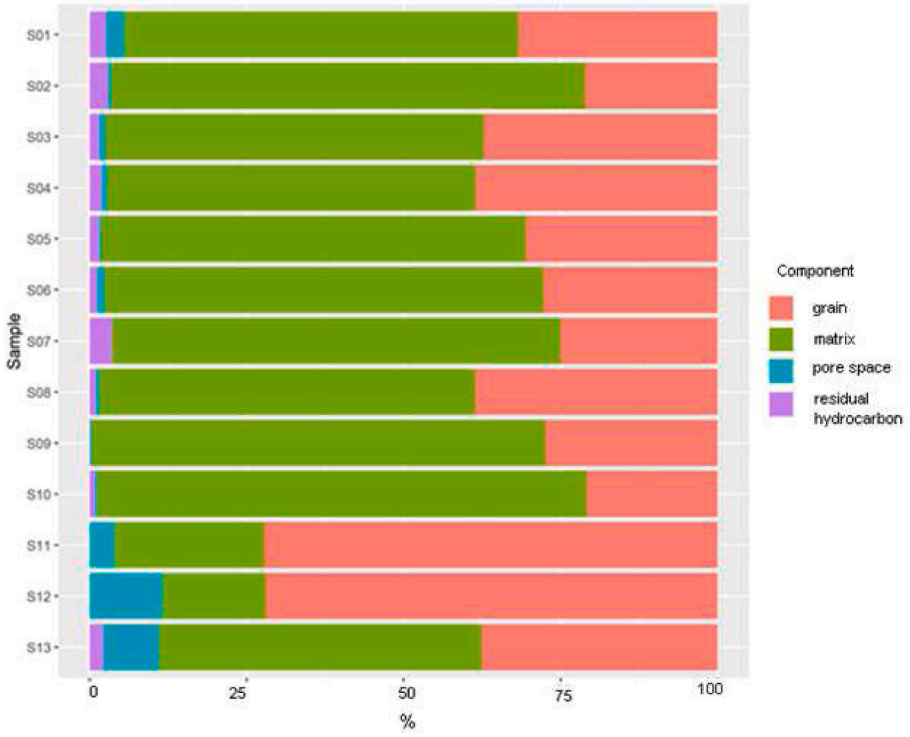

Fig. 11. Main constituents of limestone samples, OCT-X well, October Oil Field. See Table 2 for sample depths.

Table 2
Porosity and TOC values, OCT-X well, Radwany Formation, October Oil Field.

Interval	Depth (m)	Sample	Core plug		NMR[a] porosity (pu)	Mean T_2 (ms)	Visible porosity (%)	Effective porosity (wireline log-based) (%)	TOC (%)
			Permea -bility (mD)	Porosity (%)					
A	3782	S1	0.0009	1	7.7	2.21	2.95	14	
	3794	S2	0.0025	0.6	13.8	49.4	0.5	12	
	3805	S3	0.002	1	10.4	52.6	1	9	6.01
	3818	S4	0.004	0.8			0.95	12	
	3840	S5	0.008	0.7			0.3	10	2.18
	3852	S6	0.0093	1			1.1	11	3.63
	3858	S7					0.2	8	3.58
B	3925	S8					0.5	7	1.22
	3949	S9					0.3	6	2.79
	3979	S10					0.35	7	1.74
C	4013	S11					4	13	2.6
	4050	S12					11.6	11	2.45
	4100	S13					8.9	9	1.26

[a] Nuclear magnetic resonanc

drusy cement, which in turn is probably post-dated by fracture-filling blocky calcite (Fig. 9A and B).

5.1.2.2. Compaction and pressure solution. Major mechanisms for porosity destruction consisted of mechanical and chemical compaction (e.g., Choquette and Pray, 1970; Moore, 2001), the processes that generally are far more influential than cementation in porosity reduction (Ahr, 2008). The effects of compaction increased with burial depth due to increasing overburden (e.g., Schmoker and Halley, 1982; Croize et al., 2013; Husinec and Harvey, 2021). Mechanical compaction within the studied succession is evidenced by the flattened and broken foraminiferal tests, tight packing of allochems, and point contacts (Fig. 7D). It is also possible that the foraminiferal packstone texture was in part generated as a result of the closer packing of foraminifera in what originally was a wackestone. Mechanical compaction and dewatering of the initially highly porous pelagic mud (e.g., Garrison, 1981) likely began soon after burial, with significant porosity loss and thickness reduction due to dewatering, rearrangement of particles, and closer grain packing (Tucker and Wright, 1990). Following mechanical compaction during the early burial, which resulted in a stable grain framework, and subsequent late Eocene-early Oligocene uplift, further burial and the associated late-phase diagenesis resulted in the increased strain at grain contacts (Moore, 2001), and led to grain dissolution at contacts and along interfaces (e.g., Bathrust, 1975; Buxton and Sibley, 1981; Leythaeuser et al., 1995; Alsharhan and Sadd, 2000; Flügel, 2004, 2013; Husinec, 2016). These processes are evidenced in the studied succession by the presence of abundant wispy dissolution seams and stylolites, especially within foraminiferal wackestone and wackestone-packstone. Pressure solution also led to the internal redistribution of organic matter in the form of local concentrations of asphaltenes along solution seams and stylolites (Leythaeuser et al., 1995) (Fig. 10). Pressure solution likely began at depths of 200–300 m,

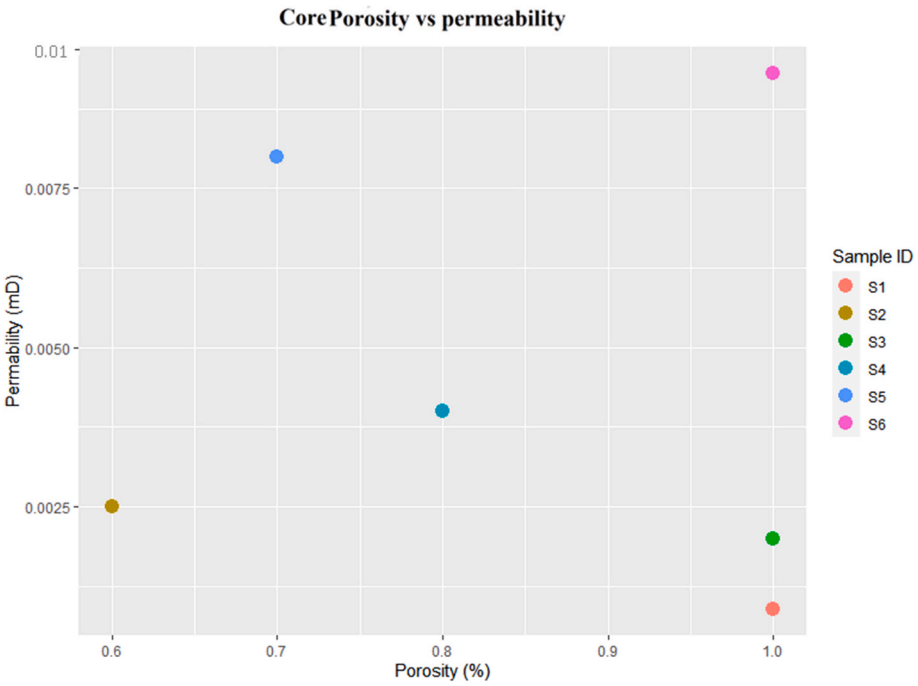

Fig. 12. Cross plot of porosity versus permeability based on limited core-plug data, OCT-X well, October Oil Field.

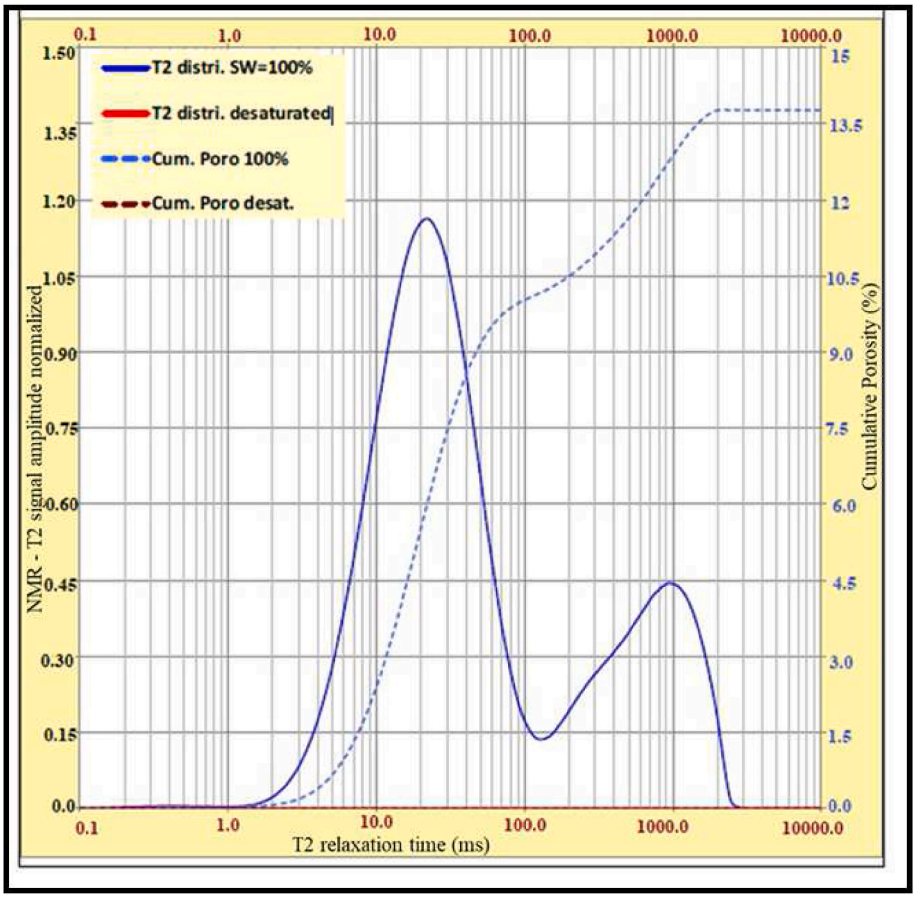

Fig. 13. Representative nuclear magnetic resonance (NMR) curve, sample S2, depth 3794 m (13,038 ft), OCT-X well, October Oil Field. T2 = transverse relaxation time.

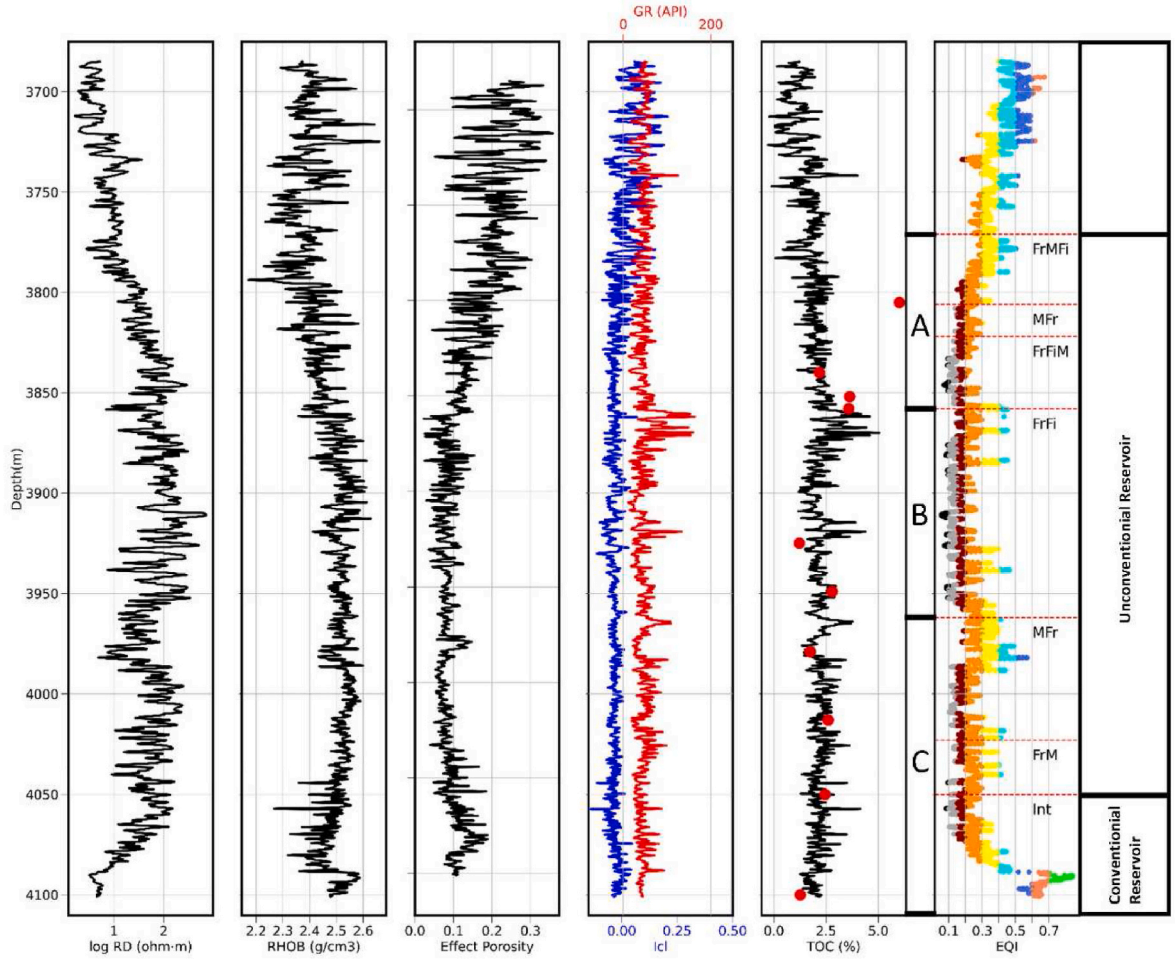

Fig. 14. Selected well logs (resistivity, density, effective porosity) and calculated logs (I_{cl}, TOC, EQI) of the Radwany Formation, OCT-X well. I_{cl} and TOC logs were calculated after Zhao et al. (2016), and EQI after Soleymanzadeh et al. (2018). EQI values are color-coded to facilitate the electrical rock classification. Porosity types: Fr = fracture, Fi = fissure, M = moldic, and Int = interparticle/intraparticle. (For interpretation of the references to color in this figure legend, the reader is referred to the Web version of this article.)

Table 3
Tortuosity (a) and cementation factor (m) for each EQI group obtained from linear fitting on a log log plot of formation factor vs. porosity.

EQI interval	a	m	R2
EQI ≤0.1	73.2	1.27	0.45
0.1 ≤ EQI ≤0.15	64.5	0.99	0.60
0.15 ≤ EQI ≤0.2	32.9	0.99	0.83
0.2 ≤ EQI ≤0.3	14.5	1.07	0.75
0.3 ≤ EQI ≤0.4	8.1	1.03	0.86
0.4 ≤ EQI ≤0.5	4.6	1.06	0.97
0.5 ≤ EQI ≤0.6	3.4	0.98	0.95
0.6 ≤ EQI ≤0.7	2.6	0.98	0.87
0.7 ≤ EQI ≤0.8	–	–	–

with the first stylolites forming at burial depths of at least 500 m (Lind, 1993; Fabricius, 2000).

5.1.2.3. Authigenic mineralization and asphaltene accumulation. Pyrite occurs as microframboids scattered within the matrix or replacing bioclasts (Fig. 9E and F) throughout the studied succession. The formation of pyrite framboids during deposition or shallow burial in deep-marine sediments requires an anaerobic environment (Schallreuter, 1984), although they can also form diagenetically during late burial, during low-grade metamorphism, and by hydrothermal alteration (Li et al., 2022). Framboid size distribution is typically fixed very early during anoxic diagenesis, generally within the top few centimeters of burial, and is preserved through advanced stages of diagenesis and lithification (Wilkin et al., 1996). The pyrite is formed as a result of sulfate reduction, and the amount of pyrite formed is limited by the rates of supply of organic matter, dissolved sulfate, and reactive iron minerals (Berner, 1984). Pyrite occurs within both matrix and bioclasts, and pyritization can therefore be considered as a porosity-reducing process within the studied succession, albeit one of limited significance.

Chertification (e.g., Gao and Land, 1991; Lawrence, 1993) resulted in the formation of chert bands and nodules by the replacement of carbonates by silica of biogenic or volcanic origin (Wise and Weaver, 1974; Maliva and Siever, 1989; Whittle and Alsharhan, 1994), most likely during shallow burial. Snavely et al. (1979) proposed that the Eocene chert was sourced from the siliceous skeletal material, whereas Keheila and El-Ayyat (1992) suggested that volcanic activity was the main source for the lower Eocene chert in the Sohag area of Upper Egypt. If the former, then molds that formed by sponge spicule dissolution were subsequently obliterated by post-chertification intergranular compaction (Maliva and Siever, 1989). In the Radwany Formation at October Oil Field, chertification contributed to a reduction in the effective porosity in Interval B carbonates.

The precipitation of asphaltenes and organic matter along stylolites, pressure solution seams, and in void spaces has resulted in porosity reduction (Figs. 9C and 10). The surface precipitation and pore plugging have consequently led to permeability impairment (e.g., Mohammed

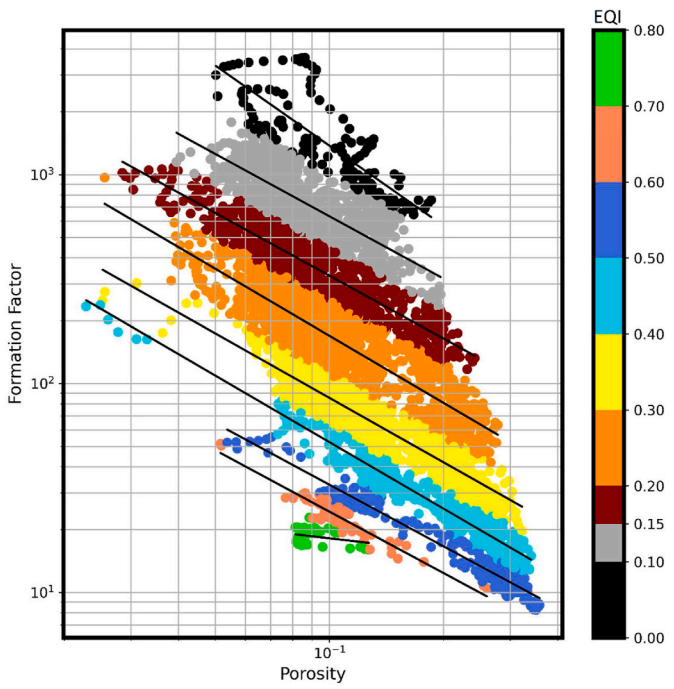

Fig. 15. Log-log plot of formation factor vs. porosity; EQI groups are color-coded. Black lines show the fitting obtained for each group. Values of tortuosity, cementation factor, and R2 are shown in Table 3. (For interpretation of the references to color in this figure legend, the reader is referred to the Web version of this article.)

et al., 2021). Since the depositional environment was in general isolated from terrestrial influences, the organic matter is most likely of marine origin (e.g., Tyson, 1995; Koch et al., 2017). Given the overall tight reservoir characteristics, stylolites likely served as primary hydrocarbon migration pathways (cf., Liu et al., 2020). Although the asphaltene-rich residues occur in moderate amounts only, they may have had a significant impact on permeability by subsequently reducing or closing the pore throats (e.g., Lomando, 1992; Al Aasm and Packard, 2000; Al-Siyabi, 2005).

5.2. Electrical quality index vs. porosity

Soleymanzadeh et al. (2018) suggested a strong correlation between EQI and the porosity efficiency and flow-pattern parameters in carbonate rocks, and applied the EQI method as an effective tool in electrical rock typing. The EQI analysis of the Radwany Formation. yielded nine groups of rock types with EQI values ranging from 0.1 to 0.8 (Fig. 15). This indicates a high heterogeneity of the formation, as the differences in transport properties and pore spaces of carbonate rocks may lead to a larger range of EQI values (Soleymanzadeh et al., 2018; Sun et al., 2021). In which case, the larger EQI values indicate higher porosity efficiency and a homogeneous flow pattern, while the lower EQI indicates lower porosity efficiency and a heterogeneous flow pattern. The highest EQI values of the Radwany Formation that were recorded in its lower Interval C, which is dominated by interparticle/intraparticle porosities, tie with the high visible and estimated porosities, and reflect low tortuosity values in the packstone microfacies of Interval C. The remaining part of Interval C, which is dominated by moldic-fracture and fracture-moldic porosity, exhibits low to moderate EQI values; moldic porosity is typically related to the lowest EQI values (Soleymanzadeh et al., 2018).

Within Interval B, several moderate EQI values (0.3–0.5) are in sharp contrast with the overall low EQI values. These are likely related to better pore connectivity given the larger number of the observed fractures. The highest EQI values characterize the last part of this interval, and correspond to the low tortuosity values resulting in a good porosity efficiency. The low EQI values of the lower and middle part of Interval A correlate with the predominance of the moldic-fracture and fracture-fissure-moldic porosity (Fig. 14); moderate values (0.3–0.5) in its upper part are compatible with the more abundant fractures.

5.3. Unconventional and conventional reservoir potential

Alsharhan (2003) identified the Radwany-equivalent Thebes Formation as both a source and a reservoir rock in the Gulf of Suez. In addition, it may serve as a seal preventing oil migration from the underlying Cretaceous sandstone reservoirs. The Radwany Formation is made up of deep-water carbonate facies (Radwan et al., 2020) that formed in an environment conducive to organic matter preservation (Michel et al., 2019; Xia et al., 2019; Boutaleb et al., 2022), as evidenced by both the geochemical measurements (Fig. 5, Table 2) and well-log TOC estimates (Fig. 14). The measured TOC values (1.22 wt % to 6 wt

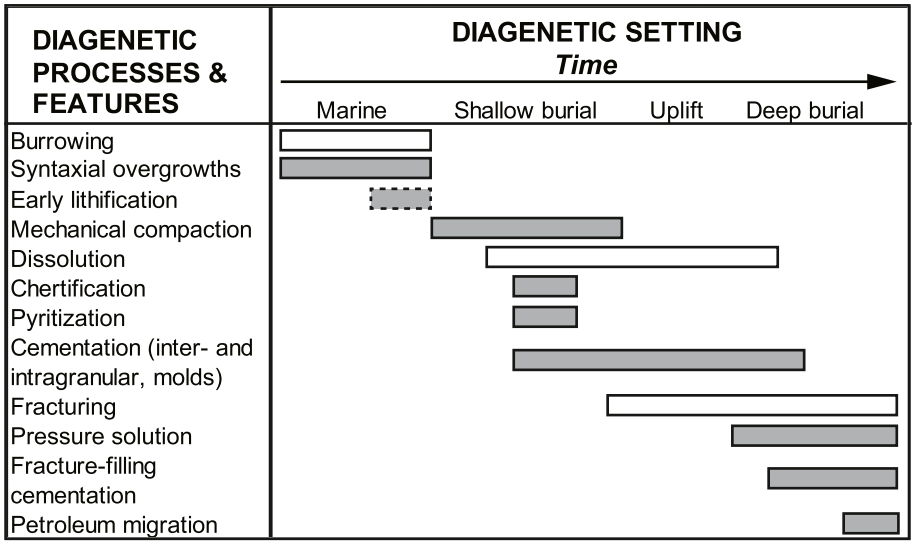

Fig. 16. Paragenetic sequence showing the timing of diagenetic processes within the Radwany Formation, October Oil Field. Porosity-enhancing processes are indicated with white bars and those reducing porosity with grey bars.

%) reflect the good to very good source rock quality (good = 1–2 wt %, very good >2%; Baskin, 1997). In addition, the continuous estimated TOC log (Fig. 14) exhibits a mean ranging between 1 wt % and 3 wt %. Overall, there is a very good correlation between the wireline-log estimated and the core-measured TOC values (Table 2 and Fig. 14). A poor correlation in the upper part of Interval A, where the highest TOC values were measured, may be partly due to the very low natural radioactivity (GR response), and partly due to the averaged values that may not be truly representative of this relatively thin source-rock unit. The EQI-based rock classification indicates a low-medium porosity efficiency for the bulk of the formation, which supports the tight nature of the formation except for its basal part. In order to better assess the unconventional reservoir potential, more geochemical analyses (i.e., pyrolysis) are needed as well as geomechanical measurements yielding information on the rock brittleness.

Regarding the pore systems, the Radwany Formation exhibits very low permeability (<0.01 mD) and poor to good porosity values (mean 7%) based on core plug measurements, thin-section analyses, and wireline-log data (Table 2, Figs. 11, 13–14). The higher values of porosity recorded by NMR reflect total porosity; movable porosity will have lower values that are closer to those mentioned above. The only part of the studied succession with conventional reservoir potential occurs at the base of the Radwany Formation. The vertical distribution of average density-neutron porosity thus shows that the highest porosity values are associated with Interval C which is composed mainly of foraminiferal packstone. Porosity in this grain-supported fabric is associated with interparticle pore spaces, and porosity loss is due to mechanical and chemical compaction. The base of the Radwany Formation (basal Interval C with interparticle/intraparticle porosities; Figs. 14 and 15) with the highest EQI values exhibits high visible and estimated porosity values. This reflects the low tortuosity values of the Interval C packstone microfacies, and its high degree of pore network connectivity compared to the middle and upper parts of Interval C with larger moldic pores (cf., Soleymanzadeh et al., 2018; Sun et al., 2021). Foraminiferal packstone also occurs in Interval A in the upper part of the formation. However, porosity in that interval is significantly reduced as a result of calcite cementation, and subordinately due to pyritization and asphaltene precipitation. The lowest visual porosity and EQI values occur in the middle part of the studied section (Interval B), which is dominated by foraminiferal wackestone. Porosity values are slightly higher in the overlying interval A where all three microfacies (packstone, wackestone, and wacke-packstone) occur. Intervals A and B are characterized by moderate to low EQI values and cementation factors (Table 3, Fig. 15), indicating reduced connectivity of the pore network, i.e., higher tortuosity (Tiab and Donaldson, 2004; Ellis and Singer, 2007; Glover, 2009). Overall, porosity in both the A and B Intervals was reduced because of the mechanical and chemical compaction along with authigenic cementation and asphaltene precipitation.

Thus, the Radwany Formation at the October Oil Field shows an unconventional reservoir potential in Interval A (and subordinately B), and a conventional potential in the lower part of Interval C. However, further regional studies are required in this under-explored section of the Gulf of Suez to fully evaluate the reservoir potential of the formation. In particular, the currently unavailable sonic velocity data, coupled with a detailed characterization of macro-to nanoscale pore architecture, geomechanical and advanced geochemical analyses, as well as the establishment of a high-resolution sequence stratigraphic framework, should enable a prediction of the key potentially producing intervals within the unconventional Interval A reservoir.

5.4. Limitations of this study and further recommendations

The results of this study suggest that the middle and upper parts of the Radwany Formation (intervals A and B) at October Oil Field have unconventional reservoir potential. However, in order to fully evaluate such a resource potential, additional research methods should be applied. Firstly, a quantitative analysis of the pore evolution process should be undertaken by utilizing the scanning electron microscopy (SEM) along the whole interval with the unconventional potential. Secondly, mechanical tests on carbonate samples should be performed in order to define the geomechanical characteristics (e.g., brittle index (BI), in-situ stress, Poisson's ratio, and Young's modulus). Namely, although the Radwany Formation is an organic-rich interval with relatively uniform distribution across the October Oil Field, the brittleness of the formation has not yet been tested or estimated. Also, although fractures have been recorded in thin sections and core samples, the fracture network is still poorly understood, and utilizing the image logs, outcrop analogs, as well as running numerical simulations should be helpful for gaining an understanding of the fracture network controls on the reservoir.

Hydraulic fracturing would be the best method for future unconventional resource exploitation, albeit it would be challenging given the burial depth of the formation. The best zones for hydraulic fracturing should be the layers with high brittleness, low in-situ stress, small horizontal stress difference, or large vertical stress difference (Fujian et al., 2019; Sohail et al., 2022). Should the above approach be successful, it would result in a major breakthrough in the deep tight oil exploration in the Gulf of Suez Basin.

6. Conclusions

At the October Oil Field, Gulf of Suez, the ~335 m (1100 feet) thick Radwany (Thebes-equivalent) Formation is composed of an Eocene (Ypresian to Lutetian) carbonate succession that can be subdivided from the base up into informal lithostratigraphic Intervals C, B, and A. Carbonates consist of organic-rich, deep-marine planktonic foraminiferal wackestone, wackestone-packstone, and packstone microfacies. By utilizing the available well logs and thin sections, coupled with petrophysical and geochemical analyses of core samples, we investigated the formation's diagenetic characteristics and evaluated its reservoir potential. The major conclusions are as follows:

1. Both fabric-selective (interparticle, intraparticle, and moldic) and non-fabric selective porosity (i.e., fractures) were identified. Interparticle porosity is dominant in the foraminiferal packstone of Interval C but is relatively rare elsewhere. Intraparticle porosity has a minor contribution to overall porosity in foraminiferal packstone and wackestone-packstone. Secondary moldic porosity is common in Intervals A and C, and most often occurs in foraminiferal wackestone and wackestone-packstone. Fractures and microfractures occur throughout the entire succession studied but are particularly abundant in foraminiferal wackestone and wackestone-packstone.
2. Porosity was enhanced by the dissolution of grains and/or lime mud matrix during early burial; later dissolution took place because of the migration of aggressive pore fluids through the carbonates. Brittle deformation had a subordinate impact on porosity; some fractures were enlarged by dissolution, although the majority of fractures were filled by calcite cement or asphaltenes during late burial.
3. The major processes contributing to porosity destruction were mechanical and chemical compaction; the latter was the source of carbonate, which was precipitated as the cement that filled pore spaces during late burial. Minor porosity-reducing processes included authigenic mineralization (pyrite, chert), and asphaltene precipitation; the latter resulted in decreased permeability by reducing or closing pore throats.
4. Core measurements and petrographic analysis indicate the tight nature of the Radwany Formation with both low permeability and porosity. Visible porosity ranges from 0.3% to 11.6% (mean 2.5%), whereas the core-plug measurements have a mean of 0.85%. Maximum values were recorded in Interval C (mean 10.2%), whereas values for Interval A (mean 1.7%) and B (mean 0.4%) are much lower. NMR analysis shows low amplitudes of short T2 components

(max. 52 ms) which indicates the presence of small pores (intraparticle, moldic, fracture, and fissure).
5. Nine EQI rock-type groups were identified, which indicates a high heterogeneity of the formation. The highest EQI values characterize the packstone microfacies in the lower Interval C which is dominated by interparticle/intraparticle porosity, and they reflect the low tortuosity values. Intervals A and B have low to moderate EQI that reflect low porosity efficiency and higher tortuosity.
6. Overall, the Radwany (Thebes) Formation at the October Oil Field has an unconventional reservoir potential in Intervals A and B (which have a TOC content of up to 6%), and conventional reservoir potential in Interval C in which the foraminiferal packstones have relatively good porosity. Such combined conventional-unconventional reservoir potential may be characteristic of similar rift-basin reservoirs elsewhere. However, a full evaluation of the reservoir potential is pending sonic velocity data, detailed characterization of the nanoscale pore architecture, and the establishment of a high-resolution sequence stratigraphic framework.
7. To fully assess the unconventional resource potential of the pelagic Eocene Limestones, a quantitative analysis of pore evolution using SEM, mechanical tests, advanced logs, outcrop analogs, and numerical simulations is required.

Declaration of competing interest

The authors declare that they have no known competing financial interests or personal relationships that could have appeared to influence the work reported in this paper.

Data availability

Data will be made available on request.

Acknowledgments

The authors are grateful to the Gulf of Suez Petroleum Company and the Egyptian General Petroleum Corporation authorities for providing the requisite data, and their permission to carry out this research. Ahmed E. Radwan is thankful for the funding provided by the Priority Research Area Anthropocene under the program “Excellence Initiative—Research University” at the Jagiellonian University in Krakow. We thank Associate Editor Hugh Daigle and two anonymous reviewers for constructive comments that greatly improved the manuscript.

References

Abdelghany, W.K., Radwan, A.E., Elkhawaga, M.A., Wood, D., Sen, S., Kassem, A.A., 2021. Geomechanical modeling using the depth-of-damage approach to achieve successful underbalanced drilling in the gulf of Suez rift basin. J. Petrol. Sci. Eng. 108311.
Abdel-Wahab, A., El-Younsy, A.R.M., 1999. Origin of spheroidal chert nodules, Drunka Formation (lower Eocene), Egypt. Sedimentology 46 (4), 733–755.
Abdullah, G., El Aal, A.A., Radwan, A.E., Qadri, T., Aly, N., 2022. The influence of carbonate textures and rock composition on durability cycles and geomechanical aspects of carbonate rocks. Acta Geotechnica 1–21.
Abudeif, A.M., Attia, M.M., Al-Khashab, H.M., Radwan, A.E., 2018. Hydrocarbon type detection using the synthetic logs: a case study, Baba member, Gulf of Suez, Egypt. J. Afr. Earth Sci. 144, 176–182.
Abudeif, A., Attia, M., Radwan, A., 2016. Petrophysical and petrographic evaluation of sidri member of belayim formation, badri field, gulf of suez, Egypt. J. Afr. Earth Sci. 115, 108–120.
Abouelresh, M.O., Mahmoud, M., Radwan, A.E., Dodd, T.J., Kong, L., Hassan, H.F., 2022. Characterization and Classification of the Microporosity in the Unconventional Carbonate Reservoirs: A Case Study from Hanifa Formation, Jafurah Basin, Saudi Arabia. Marine and Petroleum Geology, 105921.
Ahr, W.A., 2008. Geology of Carbonate Reservoirs. John Wiley & Sons.
Al-Ramadan, K., Koeshidayatullah, A., Cantrell, D., Swart, P.K., 2020. Impact of basin architecture on diagenesis and dolomitization in a fault-bounded carbonate platform: outcrop analogue of a pre-salt carbonate reservoir, Red Sea rift, NW Saudi Arabia. Petrol. Geosci. 26, 448–461.
Alsharhan, A.S., 2003. Petroleum geology and potential hydrocarbon plays in the Gulf of Suez rift basin, Egypt. AAPG (Am. Assoc. Pet. Geol.) Bull. 87, 143–180.
Alsharhan, A.S., Sadd, J.L., 2000. Stylolites in lower cretaceous carbonate reservoirs, UAE. In: Alsharhan, A.S., Scott, R.W. (Eds.), Middle East Models of Jurassic/Cretaceous Carbonate Systems, vol. 69. SEPM Special Publication, pp. 179–200.
Alsharhan, A.S., Salah, M.G., 1994. Geology and hydrocarbon habitat in rift setting: southern Gulf of Suez, Egypt. Bull. Can. Petrol. Geol. 42, 312–331.
Alsharhan, A.S., Salah, M.G., 1995. Geology and hydrocarbon habitat in rift setting: northern and central Gulf of Suez, Egypt. Bull. Can. Petrol. Geol. 43, 156–176.
Al-Siyabi, H.A., 2005. Exploration history of the Ara intrasalt carbonate stringers in the South Oman Salt Basin. GeoArabia 10, 39–72.
Amel, H., Jafarian, A., Husinec, A., Koeshidayatullah, A., Swennen, R., 2015. Microfacies, depositional environment and diagenetic evolution controls on the reservoir quality of the permian upper dalan formation, kish gas field, zagros basin. Mar. Petrol. Geol. 67, 57–71.
Appel, M., 2004. Nuclear magnetic resonance and formation porosity. Petrophysics 45, 296–307.
Aqel, M.A., 2016. Research note: permeability control on the relationship between nuclear magnetic resonance (NMR) measured porosity and routine core porosity. Arabian J. Geosci. 9 (5), 1–3.
Attia, M., Abudeif, A., Radwan, A., 2015. Petrophysical analysis and hydrocarbon potentialities of the untested middle Miocene sidri and baba sandstone of belayim formation, badri field, gulf of suez, Egypt. J. Afr. Earth Sci. 109, 120–130.
Bartlett, G.A., Greggs, R.G., 1969. Carbonate sediments: oriented lithified samples from the north atlantic. Science 166, 740–741.
Baskin, D.K., 1997. Atomic H/C ratio of kerogen as an estimate of thermal maturity and organic matter conversion. AAPG Bull. 81 (9), 1437–1450.
Bastesen, E., Rotevatn, A., 2012. Evolution and structural style of relay zones in layered limestone-shale sequences: insights from the Hammam Faraun Fault Block, Suez Rift, Egypt. J. Geol. Soc. 169, 477–488.
Bathrust, R.G.C., 1975. Carbonate Sediments and Their Diagenesis. Elsevier Science.
Benjumea, B., López, A.I., Mari, J.L., García-Lobón, J.L., 2019. Petrophysical characterization of carbonates (SE of Spain) through full wave sonic data. J. Appl. Geophys. 160, 1–14.
Berner, R.A., 1984. Sedimentary pyrite formation: an update. Geochem. Cosmochim. Acta 48, 605–615.
Biehl, B.C., Reuning, L., Schoenherr, H., Lüders, V., Kukla, P.A., 2016. Impacts of hydrothermal dolomitization and thermochemical sulfate reduction on secondary porosity creation in deeply buried carbonates: a case study from the Lower Saxony Basin, northwest Germany. AAPG (Am. Assoc. Pet. Geol.) Bull. 100, 597–621.
Bosworth, W., Mcclay, K., 2001. Structural and stratigraphic evolution of the Gulf of Suez rift, Egypt: a synthesis. Mem. Mus. Natl. Hist. Nat. 186, 567–606.
Boutaleb, K., Baouche, R., Sadaoui, M., Radwan, A.E., 2022. Sedimentological, petrophysical, and geochemical controls on deep marine unconventional tight limestone and dolostone reservoir: insights from the Cenomanian/Turonian oceanic anoxic event 2 organic-rich sediments, Southeast Constantine Basin, Algeria. Sediment. Geol. 429, 106072 https://doi.org/10.1016/j.sedgeo.2021.106072.
Bosworth, W., Khalil, S., Clare, A., Comisky, J., Abdelal, H., Reed, T., Kokkoros, G., 2014. Integration of outcrop and subsurface data during the development of a naturally fractured Eocene carbonate reservoir at the East Ras Budran concession, Gulf of Suez, Egypt. Geological Society of London Special Publication 374, 333–360.
Burchette, T.P., 2012. Carbonate rocks and petroleum reservoirs: a geological perspective from the industry. Geological Society of London Special Publication 370, 17–37.
Buxton, T.M., Sibley, D.F., 1981. Pressure solution features in a shallow buried limestone. J. Sediment. Res. 51, 19–26.
Choquette, P.W., Pray, L.C., 1970. Geologic nomenclature and classification of porosity in sedimentary carbonates. AAPG (Am. Assoc. Pet. Geol.) Bull. 54, 207–250.
Coates, G.R., Xiao, L., Prammer, M.G., 1999. NMR Logging Principles and Applications. Elsevier Science, p. 260, 755.
Corlett, H.J., Bastesen, E., Gawthorpe, R.L., Hirani, J., Hodgetts, D., Hollis, C., Rotevatn, A., 2018. Origin, dimensions, and distribution of remobilized carbonate deposits in a tectonically active zone, Eocene Thebes Formation, Sinai, Egypt. Sediment. Geol. 372, 44–63.
Croize, D., Renard, F., Gratier, J.P., 2013. Compaction and porosity reduction in carbonates: a review of observations, theory, and experiments. Adv. Geophys. 54, 181–238 (Elsevier).
Darwish, M., El-Araby, A.M., 1993. Petrography and diagenetic aspects of some siliciclastic hydrocarbon reservoirs in relation to the rifting of the Gulf of Suez. In: Philobbos, E.R., Purser, B.H. (Eds.), Geodynamics and Sedimentation of the Red Sea–Gulf of Aden Rift System, vol. 1. Geological Society of Egypt Special Publication, pp. 155–187.
Dolson, J., 2020. The petroleum geology of Egypt and history of exploration. In: The Geology of Egypt. Springer, Cham, pp. 635–658.
Dolson, J.C., Atta, M., Blanchard, D., Sehim, A., Villinski, J., Loutit, T., Romine, K., 2014. Egypt's future petroleum resources: a revised look in the 21st Century. In: Marlow, L., Kendall, C., Yose, L. (Eds.), Petroleum Systems of the Tethyan Region, vol. 106. AAPG Memoir, pp. 143–178.
Dolson, J.C., Shann, M.V., Matbouly, S.I., Hammouda, H., Rashed, R.M., 2001. Egypt in the twenty-first century: petroleum potential in offshore trends. GeoArabia 6, 211–230.
Dunham, R.J., 1962. Classification of carbonate rocks according to depositional textures. AAPG (Am. Assoc. Pet. Geol.) Bull. 1, 108–121.
Eberli, G.P., Baechle, G.T., Anselmetti, F.S., Incze, M.L., 2003. Factors controlling elastic properties in carbonate sediments and rocks. Lead. Edge 22 (7), 654–660.
Egpc, 1996. Gulf of Suez Oil Fields (A Comprehensive Overview). Egyptian General Petroleum Corporation, Cairo.

Ehrenberg, S.N., Walderhaug, O., 2015. Preferential calcite cementation of macropores in microporous limestones. J. Sediment. Res. 85, 780–793.
Ehrenberg, S.N., Walderhaug, O., Bjørlykke, K., 2012. Carbonate porosity creation by mesogenetic dissolution: reality or illusion? AAPG (Am. Assoc. Pet. Geol.) Bull. 96, 217–233.
Ehrenberg, S.N., Walderhaug, O., Bjørlykke, K., 2019. Discussion of "Microfacies, diagenesis and oil emplacement of the Upper Jurassic Arab-D carbonate reservoir in an oil field in central Saudi Arabia (Khurais Complex)" by Rosales et al. Mar. Petrol. Geol. 100, 551–553, 2018.
El Baz, S.M., Kassem, A.A., 2020. The Cenomanian-Turonian boundary event in Egypt: foraminiferal turnover and carbon isotopic change. Rev. Micropaleontol. 69, 100463.
El Diasty, W.S., El Beialy, S.Y., Mostafa, A.R., Ghonaim, A.A., Peters, K.E., 2020. Chemometric differentiation of oil families and their potential source rocks in the gulf of suez. Nat. Resour. Res. 29, 2063–2102.
El-Ghamri, M.A., Warburton, I.C., Burley, S.D., 2002. Hydrocarbon generation and charging in the october field, gulf of suez, Egypt. J. Petrol. Geol. 25, 433–464.
Elsayed, M., Isah, A., Hiba, M., Hassan, A., Al-Garadi, K., Mahmoud, M., et al., 2022. A review on the applications of nuclear magnetic resonance (NMR) in the oil and gas industry: laboratory and field-scale measurements. J. Pet. Explor. Prod. Technol. 1–38.
Ellis, D.V., Singer, J.M., 2007. Well Logging for Earth Scientists. Springer Netherlands.
El-Shahat, W., Villinski, J.C., El-Bakry, G., 2009. Hydrocarbon potentiality, burial history and thermal evolution for some source rocks in October oil field, northern Gulf of Suez, Egypt. J. Petrol. Sci. Eng. 68, 245–267.
Fabricius, I.L., 2000. Interpretation of burial history and rebound from loading experiments and occurrence of microstylolites in mixed sediments of Caribbean Sites 999 and 1001. In: Leckie, R.M., Sigurdson, H., Acton, G.D., Draper, G. (Eds.), Proceedings of the Ocean Drilling Program, vol. 165. Scientific Results, pp. 177–190.
Fallah-Bagtash, R., Jafarian, A., Husinec, A., Adabi, M.A., 2020. Diagenetic stabilization of the upper permian dalan formation, Persian gulf basin. J. Asian Earth Sci. 189, 104144.
Fischer, A.G., Garrison, R.E., 1967. Carbonate lithification on the sea floor. J. Geol. 75, 488–496.
Flügel, E., 2004. Microfacies of Carbonate Rocks Analysis. Analysis, Interpretation and Application. Springer-Verlag, Berlin Heideberg, New York.
Fujian, Z.H.O.U., Hang, S.U., Liang, X., Leifeng, M.E.N.G., Lishan, Y.U.A.N., Xiuhui, L.I., Liang, T., 2019. Integrated hydraulic fracturing techniques to enhance oil recovery from tight rocks. Petrol. Explor. Dev. 46 (5), 1065–1072.
Föllmi, K.B., Von Breymann, M.T., 1992. Phosphates and glauconites of sites 798 and 799. In: Pisciotto, K.A., Ingle, J.C., von Breymann, M.T., Barron, J., et al. (Eds.), Proceedings of the Ocean Drilling Program, Scientific Results, vol. 127. Ocean Drilling Program), College Station, TX, pp. 63–74.
Gao, G., Land, L.S., 1991. Nodular chert from the Arbuckle Group, Slick Hills, SW Oklahoma: a combined field, petrographic and isotopic study. Sedimentology 38, 857–870.
Garrison, R.E., 1981. Diagenesis of Oceanic Carbonate Sediments; a Review of the DSDP Perspective, vol. 32. SEPM Special Publication, pp. 181–207.
Ghasemi, M., Kakemem, U., Husinec, A., 2022. Automated approach to reservoir zonation: a case study from the Upper Permian Dalan (Khuff) carbonate ramp, Persian Gulf. J. Nat. Gas Sci. Eng. 97, 104332.
Glover, P.W.J., 2009. What is the cementation exponent? A new interpretation. Lead. Edge 28, 82–85.
Gubelin, G., Boyd, A., 1997. Total porosity and bound-fluid measurements from an NMR tool. J. Petrol. Technol. 49, 718. SPE 39096).
Guiraud, R., Bosworth, W., Thierry, J., Delplanque, A., 2005. Phanerozoic geological evolution of northern and central africa: an overview. J. Afr. Earth Sci. 43, 83–143.
GUPCO, 2020. Reegional geomechanical database validations in the gulf of suez region. Internal Report.
Hesse, R., 1989. Silica diagenesis: origin of inorganic and replacement cherts. Earth Sci. Rev. 26 (1), 253–284.
Hollis, C., 2011. Diagenetic controls on reservoir properties of carbonate successions within the Albian-Turonian of the Arabian Plate. Petrol. Geosci. 17, 223–241.
Hollis, C., Lawrence, D.A., De Perière, M.D., Al Darmaki, F., 2017. Controls on porosity preservation within a Jurassic oolitic reservoir complex, UAE. Mar. Petrol. Geol. 88, 888–906.
Husinec, A., 2016. Sequence stratigraphy of the red river formation, Williston basin, USA: stratigraphic signature of the ordovician katian greenhouse to icehouse transition. Mar. Petrol. Geol. 77, 487–506.
Husinec, A., Harvey, L.A., 2021. Late Ordovician climate and sea-level record in a mixed carbonate-siliciclastic-evaporite lithofacies, Williston Basin. Palaeogeogr. Palaeoclimatol. Palaeoecol. 561, 110054. USA.
Hussein, A.W., Abd El-Rahman, Y.M., 2020. Origin of chert within the turonian carbonates of abu roash formation, abu roash area, Egypt: field, petrographic, and geochemical perspectives. Geol. J. 55, 2805–2833.
Kakemem, U., Jafarian, A., Husinec, A., Adabi, M.H., Mahmoudi, A., 2021. Facies, sequence framework, and reservoir quality along a triassic carbonate ramp: kangan formation, south pars field, Persian gulf superbasin. J. Petrol. Sci. Eng. 198, 108166.
Kassem, A.A., Sharaf, L.M., Baghdady, A.R., El-Naby, A.A., 2020. Cenomanian/Turonian oceanic anoxic event 2 in October oil field, central Gulf of Suez, Egypt. J. Afr. Earth Sci. 165, 103817.
Kassem, A.A., Hussein, W.S., Radwan, A.E., Anani, N., Abioui, M., Jain, S., Shehata, A.A., 2021. Petrographic and diagenetic study of siliciclastic jurassic sediments from the northeastern margin of africa: implication for reservoir quality. J. Petrol. Sci. Eng. 200, 108340.
Keheila, E.A., El-Ayyat, A., 1992. Silicification and dolomitization of the lower Eocene carbonates in the Eastern Desert between Sohag and qena, Egypt. J. Afr. Earth Sci. 14, 341–349.
Koch, G., Prtoljan, B., Husinec, A., Hajek-Tadesse, V., 2017. Palynofacies and paleoenvironment of the Upper Jurassic mud-supported carbonates, southern Croatia: preliminary evaluation of the hydrocarbon source rock potential. Mar. Petrol. Geol. 80, 243–253.
Lawrence, M.J., 1993. Sedimentology and petrography of early diagenetic chert and dolomite in the late cretaceous-early tertiary amuri limestone group, eastern Marlborough, New Zealand. N. Z. J. Geol. Geophys. 36, 9–25.
Leythaeuser, D., Borromeo, O., Mosca, F., Di Primio, R., Radke, M., Schaefer, R.G., 1995. Pressure solution in carbonate source rocks and its control on petroleum generation and migration. Mar. Petrol. Geol. 12, 717–733.
Li, K., Huang, F., Gao, S., Zhang, Z., Ren, Y., An, B., 2022. Morphology of framboidal pyrite and its textural evolution: evidence from the Logatchev area, Mid-Atlantic Ridge. Ore Geol. Rev. 141, 104630.
Lind, I.L., 1993. Stylolites in chalk from Leg 130, ontong java plateau. In: Berger, W.H., Kroenke, J.W., Mayer, L.A. (Eds.), Proceedings of the Ocean Drilling Program, vol. 130. Scientific Results, pp. 445–451.
Liu, S., Gao, G., Gang, W., Qu, W., Dang, W., Zhang, W., Yang, S., Zhu, K., 2020. Implications of organic matter source and fluid migration from geochemical characteristics of stylolites and matrix in carbonate rocks: a case study from the Carboniferous and the Ordovician in the Sichuan Basin, SW China. J. Petrol. Sci. Eng. 186, 106606.
Lomando, A.J., 1992. The influence of solid reservoir bitumen on reservoir quality. AAPG (Am. Assoc. Pet. Geol.) Bull. 76, 1137–1152.
Lucia, F.J., 2007. Carbonate Reservoir Characterization - an Integrated Approach. Springer-Verlag, Berlin-Heidelberg.
Machel, H.G., 2001. Bacterial and thermochemical sulfate reduction in diagenetic settings - old and new insights. Sediment. Geol. 140, 143–175.
Machel, H., 2005. Investigations of burial diagenesis in carbonate hydrocarbon reservoir rocks. Geosci. Can. 32, 103–128.
Maliva, R.G., Siever, R., 1989. Nodular chert formation in carbonate rocks. J. Geol. 97, 421–433.
Matter, A., Douglas, R.G., Perch-Nielsen, K., 1975. Fossil preservation, geochemistry, and diagenesis, of pelagic carbonates from shatsky rise, northwest pacific. Deep Sea Drilling Project 32, 891–921. *Initial reports of the*.
Mcclay, K.R., Nichols, G.J., Khalil, S.M., Darwish, M., Bosworth, W., 1998. Extensional tectonics and sedimentation, eastern Gulf of Suez, Egypt. In: Purser, B.H., Bosence, D.W.J. (Eds.), Sedimentation and Tectonics in Rift Basins, Red Sea - Gulf of Aden. Springer, Dordrecht, pp. 223–238.
Michel, J., Laugié, M., Pohl, A., Lanteaume, C., Masse, J.P., Donnadieu, Y., Borgomano, J., 2019. Marine carbonate factories: a global model of carbonate platform distribution. Int. J. Earth Sci. 108 (6), 1773–1792.
Moore, C.H., 2001. Carbonate reservoirs: porosity and diagenesis in a sequence stratigraphic framework. Dev. Sedimentol. 55.
Mostafa, A.R., Klitzsch, E., Matheis, G., Ganz, H., 1993. Origin and evaluation of hydrocarbons in the gulf of Suez Basin, Egypt. In: Thorweihe, U., Schandelmeier, H. (Eds.), Geoscientific Research in North East Africa, pp. 267–275. Rotterdam, Balkema.
Moustafa, A.R., Khalil, S.M., 2020. Structural setting and tectonic evolution of the gulf of suez, NW red sea and gulf of aqaba rift systems. In: Hamimi, Z., El-Barkooky, A., Martínez Frías, J., Fritz, H., Abd El-Rahman, Y. (Eds.), The Geology of Egypt. Regional Geology Reviews. Springer, Cham, pp. 295–342.
Nelson, R.A., 2001. Evaluating fractured reservoirs. Geologic Analysis of Naturally Fractured Reservoirs 1–100.
Patton, T.L., Moustafa, A.R., Nelson, R.A., Abdine, S.A., 1994. Tectonic evolution and structural setting of the Suez Rift. In: Landon, S.M. (Ed.), Interior Rift Basins, vol. 59. American Association of Petroleum Geologists Memoir, pp. 7–55.
Pettijohn, F.J., Potter, P.E., Siever, R., 1973. Sand and Sandstones. Springer-Verlang, Berlin.
Radwan, A.E., 2021. Modeling the depositional environment of the sandstone reservoir in the middle Miocene sidri member, badri field, gulf of Suez Basin, Egypt: integration of gamma-ray log patterns and petrographic characteristics of Lithology. Nat. Resour. Res. 30, 431–449.
Radwan, A.E., Trippetta, F., Kassem, A.A., Kania, M., 2021a. Multi-scale characterization of unconventional tight carbonate reservoir: insights from October oil filed, Gulf of Suez rift basin, Egypt. J. Petrol. Sci. Eng. 197, 107968.
Radwan, A.E., Nabawy, B.S., Kassem, A.A., Hussein, W.S., 2021b. Implementation of Rock Typing on Waterflooding Process during Secondary Recovery in Oil Reservoirs: A Case Study, El Morgan Oil Field, Gulf of Suez, Egypt. *Natural Resources Research*. https://doi.org/10.1007/s11053-020-09806-0.
Radwan, A.E., Kassem, A.A., Kassem, A., 2020c. Radwany Formation: a new formation name for the Early-Middle Eocene carbonate sediments of the offshore October oil field, Gulf of Suez: contribution to the Eocene sediments in Egypt. Mar. Petrol. Geol. 116, 104304.
Radwan, A.E., 2022. A multi-proxy approach to detect the pore pressure and the origin of overpressure in sedimenatry basins: An example from the Gulf of Suez Rift Basin. Front. Earth Sci. 1607 https://doi.org/10.3389/feart.2022.967201.
Radwan, A.E., Abudeif, A.M., Attia, M.M., 2020b. Investigative petrophysical fingerprint technique using conventional and synthetic logs in siliciclastic reservoirs: a case study, Gulf of Suez basin, Egypt. J. Afr. Earth Sci. 167, 103868.
Radwan, A.E., Abudeif, A.M., Attia, M.M., Elkhawaga, M.A., Abdelghany, W.K., Kasem, A.A., 2020a. Geopressure evaluation using integrated basin modelling, well-logging and reservoir data analysis in the northern part of the Badri oil field, Gulf of Suez, Egypt. J. Afr. Earth Sci. 162, 103743.

Radwan, A.E., Abudeif, A.M., Attia, M.M., Mahmoud, M.A., 2019a. Development of formation damage diagnosis workflow, application on Hammam Faraun reservoir: a case study, Gulf of Suez, Egypt. J. Afr. Earth Sci. 153, 42–53.
Radwan, A.E., Abudeif, A., Attia, M., Mahmoud, M., 2019b. Development of formation damage diagnosis workflow, application on Hammam Faraun reservoir: a case study, Gulf of Suez, Egypt. In: Offshore Mediterranean Conference. ISBN9788894043679-2019.
Radwan, A.E., Abudeif, A.M., Attia, M.M., Mohammed, M.A., 2019c. Pore and fracture pressure modeling using direct and indirect methods in Badri Field, Gulf of Suez, Egypt. J. Afr. Earth Sci. 156, 133–143.
Read, J.F., Husinec, A., Cangialosi, M., Loehn, C.W., Prtoljan, B., 2016. Climate controlled, fabric destructive, reflux dolomitization and stabilization via marine- and synorogenic mixed fluids: an example from a large Mesozoic, calcite-sea platform, Croatia. Palaeogeogr. Palaeoclimatol. Palaeoecol. 449, 108–126.
Reineck, H.E., 1963. Sedimentgefüge im Bereich der südlichen Nordsee. Abhandlungen der Senckenbergischen Naturforschenden Gesellschaft. Band 505, 138.
Robson, D.A., 1971. The structure of the Gulf of Suez (Clysmic) rift, with special reference to the eastern side. J. Geol. Soc. 127, 247–271.
Roduit, N., 2020. JMicroVision: Image Analysis Toolbox for Measuring and Quantifying Components of High-Definition Images. Version 1.3.1 accessed 7 April 2020.
Rotevatn, A., Bastesen, E., 2014. Fault Linkage and Damage Zone Architecture in Tight Carbonate Rocks in the Suez Rift (Egypt): Implications for Permeability Structure along Segmented Normal Faults, vol. 374. Geological Society of London Special Publication, pp. 79–95.
Said, R., 1960. Planktonic foraminifera from the Thebes Formation, Luxor, Egypt. Micropaleontology 6, 277.
Said, R., 1962. The Geology of Egypt. Elsevier, Amsterdam, p. 377.
Said, R., 2017. The Geology of Egypt. Routledge, p. 734.
Schallreuter, R., 1984. Framboidal pyrite in deep-sea sediments. DSDP Initial Reports 75, 875–891.
Scheibner, C., Marzouk, A.M., Kuss, J., 2001. Maastrichtian-Early Eocene litho-biostratigraphy and palægeography of the northern Gulf of Suez region, Egypt. J. Afr. Earth Sci. 32, 223–255.
Schmoker, J.W., Halley, R.B., 1982. Carbonate porosity versus depth - a predictable relation to south Florida. AAPG (Am. Assoc. Pet. Geol.) Bull. 66, 2561–2570.
Shaaban, M.N., 2004. Diagenesis of the lower Eocene Thebes Formation, Gebel rewagen area, Eastern Desert, Egypt. Sediment. Geol. 165, 53–65.
Shehata, A.A., Kassem, A.A., Brooks, H.L., Zuchuat, V., Radwan, A.E., 2021. Facies Analysis and Sequence-Stratigraphic Control on Reservoir Architecture: Example from Mixed Carbonate/siliciclastic Sediments of Raha Formation, Gulf of Suez, Egypt. Marine and Petroleum Geology, 105160.
Snavely, P.D., Garrison, R.E., Meguid, A.A., 1979. Stratigraphy and regional depositional history of the Thebes Formation (lower Eocene), Egypt. Ann. Geol. Surv. Egypt 9, 344–362.
Sohail, Ghulam Mohyuddin, Radwan, Ahmed E., Mahmoud, Mohamed, 2022. A review of Pakistani shales for shale gas exploration and comparison to North American shale plays. Energy Rep. 8, 6423–6442.
Soleymanzadeh, A., Jamialahmadi, M., Helalizadeh, A., Soulgani, B.S., 2018. A new technique for electrical rock typing and estimation of cementation factor in carbonate rocks. J. Petrol. Sci. Eng. 166, 381–388.
Steckler, M.S., Berthelot, F., Lyberis, N., Le Pichon, X., 1988. Subsidence in the Gulf of Suez: implications for rifting and plate kinematics. Tectonophysics 153, 249–270.
Sun, Z., Mehmani, A., Torres-Verdín, C., 2021. Pore-scale investigation of the electrical resistivity of saturated porous Media: flow patterns and porosity efficiency. J. Geophys. Res. Solid Earth 126 (12) e2021JB022608.
Taylor, A.M., Goldring, R., 1993. Description and analysis of bioturbation and ichnofabric. J. Geol. Soc. 150, 141–148.
Tiab, D., Donaldson, E.C., 2004. Petrophysics: Theory and Practice of Measuring Reservoir Rock and Fluid Transport Properties. Gulf Professional Publishing, Elsevier, Oxford.
Tucker, M.E., Wright, V.P., 1990. Carbonate Sedimentology. Blackwell Science, London.
Tyson, R.V., 1995. Sedimentary Organic Matter. Organic Facies and Palynofacies. Chapman & Hall, London.
Westphal, H., Surholt, I., Kiesl, C., Thern, H.F., Kruspe, T., 2005. NMR measurements in carbonate rocks: problems and an approach to a solution. Pure Appl. Geophys. 162, 549–570.
Whittle, G.L., Alsharhan, A.S., 1994. Dolomitization and chertification of the early Eocene rus Formation in abu dhabi, United Arab Emirates. Sediment. Geol. 92, 273–285.
Wilkin, R.T., Barnes, H.L., Brantley, S.L., 1996. The size distribution of framboidal pyrite in modern sediments: an indicator of redox conditions. Geochem. Cosmochim. Acta 60, 3897–3912.
Wise, S.W., Weaver, F.M., 1974. Chertification of Oceanic Sediments, vol. 1. International Association of Sedimentologists Special Publication, pp. 301–326.
Worden, R.H., Armitage, P.J., Butcher, A.R., Churchill, J.M., Csoma, A.E., Hollis, C., Lander, R.H., Omma, J.E., 2018. Petroleum Reservoir Quality Prediction: Overview and Contrasting Approaches from Sandstone and Carbonate Communities, vol. 435. Geological Society of London Special Publication, pp. 1–31.
Xia, L.W., Cao, J., Wang, M., Mi, J.L., Wang, T.T., 2019. A review of carbonates as hydrocarbon source rocks: basic geochemistry and oil-gas generation. Petrol. Sci. 16 (4), 713–728.
Zhao, P., Mao, Z., Huang, Z., Zhang, C., 2016. A new method for estimating total organic carbon content from well logs. AAPG (Am. Assoc. Pet. Geol.) Bull. 100, 1311–1327.